

CERN-PH-EP/2013-188
2019/06/20

CMS-HIG-13-012

Search for the standard model Higgs boson produced in association with a W or a Z boson and decaying to bottom quarks

The CMS Collaboration*

Abstract

A search for the standard model Higgs boson (H) decaying to $b\bar{b}$ when produced in association with a weak vector boson (V) is reported for the following channels: $W(\mu\nu)H$, $W(e\nu)H$, $W(\tau\nu)H$, $Z(\mu\mu)H$, $Z(ee)H$, and $Z(\nu\nu)H$. The search is performed in data samples corresponding to integrated luminosities of up to 5.1 fb^{-1} at $\sqrt{s} = 7 \text{ TeV}$ and up to 18.9 fb^{-1} at $\sqrt{s} = 8 \text{ TeV}$, recorded by the CMS experiment at the LHC. An excess of events is observed above the expected background with a local significance of 2.1 standard deviations for a Higgs boson mass of 125 GeV, consistent with the expectation from the production of the standard model Higgs boson. The signal strength corresponding to this excess, relative to that of the standard model Higgs boson, is 1.0 ± 0.5 .

Published in Physical Review D as [doi:10.1103/PhysRevD.89.012003](https://doi.org/10.1103/PhysRevD.89.012003).

1 Introduction

At the Large Hadron Collider (LHC), the ATLAS and CMS collaborations have reported the discovery of a new boson [1, 2] with a mass, m_H , near 125 GeV and properties compatible with those of the standard model (SM) Higgs boson [3–8]. To date, significant signals have been observed in channels where the boson decays into $\gamma\gamma$, ZZ , or WW . The interaction of this boson with the massive W and Z vector bosons indicates that it plays a role in electroweak symmetry breaking. The interaction with the fermions and whether the Higgs field serves as the source of mass generation in the fermion sector, through a Yukawa interaction, remains to be firmly established.

At $m_H \approx 125$ GeV the standard model Higgs boson decays predominantly into a bottom quark-antiquark pair ($b\bar{b}$) with a branching fraction of $\approx 58\%$ [9]. The observation and study of the $H \rightarrow b\bar{b}$ decay, which involves the direct coupling of the Higgs boson to down-type quarks, is therefore essential in determining the nature of the newly discovered boson. The measurement of the $H \rightarrow b\bar{b}$ decay will be the first direct test of whether the observed boson interacts as expected with the quark sector, as the coupling to the top quark has only been tested through loop effects.

In their combined search for the SM Higgs boson [10], the CDF and D0 collaborations at the Tevatron $p\bar{p}$ collider have reported evidence for an excess of events in the 115–140 GeV mass range, consistent with the mass of the Higgs boson observed at the LHC. In that search, the sensitivity below a mass of 130 GeV is dominated by the channels in which the Higgs boson is produced in association with a weak vector boson and decaying to $b\bar{b}$ [11]. The combined local significance of this excess is reported to be 3.0 standard deviations at $m_H = 125$ GeV, while the expected local significance is 1.9 standard deviations. At the LHC, a search for $H \rightarrow b\bar{b}$ by the ATLAS experiment using data samples corresponding to an integrated luminosity of 4.7 fb^{-1} at $\sqrt{s} = 7$ TeV resulted in exclusion limits on Higgs boson production, at the 95% confidence level (CL), of 2.5 to 5.5 times the standard model cross section in the 110–130 GeV mass range [12].

This article reports on a search at the Compact Muon Solenoid (CMS) experiment for the standard model Higgs boson in the $pp \rightarrow VH$ production mode, where V is either a W or a Z boson and $H \rightarrow b\bar{b}$. The previous Higgs boson search in this production mode at CMS used data samples corresponding to integrated luminosities of up to 5.1 fb^{-1} at $\sqrt{s} = 7$ TeV and up to 5.3 fb^{-1} at $\sqrt{s} = 8$ TeV [13]. The results presented here combine the analysis of the 7 TeV data sample in Ref. [13]

with an updated analysis of the full 8 TeV data sample corresponding to a luminosity of up to 18.9 fb^{-1} .

The following six channels are considered in the search: $W(\mu\nu)H$, $W(e\nu)H$, $W(\tau\nu)H$, $Z(\mu\mu)H$, $Z(ee)H$, and $Z(\nu\nu)H$, all with the Higgs boson decaying to $b\bar{b}$. Throughout this article the term “lepton” refers only to charged leptons and the symbol ℓ is used to refer to both muons and electrons, but not to taus. For the $W(\tau\nu)H$ final state, only the 8 TeV data are included and only taus with 1-prong hadronic decays are explicitly considered; the τ notation throughout this article refers exclusively to such decays. The leptonic decays of taus in WH processes are implicitly accounted for in the $W(\mu\nu)H$ and $W(e\nu)H$ channels. Backgrounds arise from production of W and Z bosons in association with jets (from gluons and from light- or heavy-flavor quarks), singly and pair-produced top quarks ($t\bar{t}$), dibosons, and quantum chromodynamics (QCD) multijet processes.

Simulated samples of signal and background events are used to provide guidance in the optimization of the analysis. Control regions in data are selected to adjust the event yields from simulation for the main background processes in order to estimate their contribution in the signal region. These regions also test the accuracy of the modeling of kinematic distributions in the simulated samples.

Upper limits at the 95% CL on the $pp \rightarrow VH$ production cross section times the $H \rightarrow b\bar{b}$ branching fraction are obtained for Higgs boson masses in the 110–135 GeV range. These limits are extracted by fitting the shape of the output distribution of a boosted-decision-tree (BDT) discriminant [14, 15]. The results of the fitting procedure allow to evaluate the presence of a Higgs boson signal over the expectation from the background components. The significance of any excess of events, and the corresponding event yield, is compared with the expectation from a SM Higgs boson signal.

2 Detector and simulated samples

A detailed description of the CMS detector can be found elsewhere [16]. The momenta of charged particles are measured using a silicon pixel and strip tracker that covers the pseudorapidity range $|\eta| < 2.5$ and is immersed in a 3.8 T axial magnetic field. The pseudorapidity is defined as $\eta = -\ln[\tan(\theta/2)]$, where θ is the polar angle of the trajectory of a particle with respect to the direction of the counterclockwise proton beam. Surrounding the tracker are a crystal electromagnetic calorimeter (ECAL) and a brass/scintillator hadron calorimeter (HCAL),

both used to measure particle energy deposits and consisting of a barrel assembly and two endcaps. The ECAL and HCAL extend to a pseudorapidity range of $|\eta| < 3.0$. A steel/quartz-fiber Cherenkov forward detector extends the calorimetric coverage to $|\eta| < 5.0$. The outermost component of the CMS detector is the muon system, consisting of gas-ionization detectors placed in the steel return yoke of the magnet to measure the momenta of muons traversing through the detector. The two-level CMS trigger system selects events of interest for permanent storage. The first trigger level, composed of custom hardware processors, uses information from the calorimeters and muon detectors to select events in less than $3.2 \mu\text{s}$. The high-level trigger software algorithms, executed on a farm of commercial processors, further reduce the event rate using information from all detector subsystems. The variable $\Delta R = \sqrt{(\Delta\eta)^2 + (\Delta\phi)^2}$ is used to measure the separation between reconstructed objects in the detector, where ϕ is the angle (in radians) of the trajectory of the object in the plane transverse to the direction of the proton beams.

Simulated samples of signal and background events are produced using various Monte Carlo (MC) event generators, with the CMS detector response modeled with GEANT4 [17]. The Higgs boson signal samples are produced using the POWHEG [18] event generator. The MADGRAPH 5.1 [19] generator is used for the diboson, W+jets, Z+jets, and $t\bar{t}$ samples. The single-top-quark samples, including the tW -, t -, and s -channel processes, are produced with POWHEG and the QCD multijet samples with PYTHIA 6.4 [20]. The production cross sections for the diboson and $t\bar{t}$ samples are rescaled to the cross sections from the next-to-leading-order (NLO) MCFM generator [21], while the cross sections for the W+jets and Z+jets samples are rescaled to next-to-next-to-leading order (NNLO) cross sections calculated using the FEWZ program [22–24]. The default set of parton distribution functions (PDF) used to produce the NLO POWHEG samples is the NLO MSTW2008 set [25], while the leading-order (LO) CTEQ6L1 set [26] is used for the other samples. For parton showering and hadronization the POWHEG and MADGRAPH samples are interfaced with HERWIG ++ [27] and PYTHIA, respectively. The PYTHIA parameters for the underlying event description are set to the Z2 tune for the 7 TeV samples and to the Z2* tune for the 8 TeV samples [28]. The TAUOLA [29] library is used to simulate tau decays.

During the 2011 data-taking period the LHC instantaneous luminosity reached up to $3.5 \times 10^{33} \text{ cm}^{-2} \text{ s}^{-1}$ and the average number of pp interactions per bunch crossing was approximately nine. During the 2012 period the LHC instantaneous luminosity reached $7.7 \times 10^{33} \text{ cm}^{-2} \text{ s}^{-1}$ and the average number of pp interac-

tions per bunch crossing was approximately twenty-one. Additional simulated pp interactions overlapping with the event of interest in the same bunch crossing, denoted as pileup events, are therefore added in the simulated samples to reproduce the pileup distribution measured in data.

3 Triggers

Several triggers are used to collect events consistent with the signal hypothesis in the six channels under consideration.

For the $W(\mu\nu)H$ and $W(e\nu)H$ channels, the trigger paths consist of several single-lepton triggers with tight lepton identification. Leptons are also required to be isolated from other tracks and calorimeter energy deposits to maintain an acceptable trigger rate. For the $W(\mu\nu)H$ channel and for the 2011 data, the trigger thresholds for the muon transverse momentum, p_T , are in the range of 17 to 24 GeV. The higher thresholds are used for the periods of higher instantaneous luminosity. For the 2012 data the muon trigger p_T threshold for the single-isolated-muon trigger is set at 24 GeV. For both the 2011 and 2012 data, a single-muon trigger with a 40 GeV p_T threshold, but without any isolation requirements, is also used for this channel. The combined single-muon trigger efficiency is $\approx 90\%$ for $W(\mu\nu)H$ events that pass all offline requirements that are described in Section 5.

For the $W(e\nu)H$ channel and for the 2011 data, the electron p_T threshold ranges from 17 to 30 GeV. To maintain acceptable trigger rates during the periods of high instantaneous luminosity, the lower-threshold triggers also require two central ($|\eta| < 2.6$) jets, with a p_T threshold in the 25–30 GeV range, and a minimum requirement on the value of an online estimate of the missing transverse energy, E_T^{miss} , in the 15–25 GeV range. E_T^{miss} is defined online as the magnitude of the vector sum of the transverse momenta of all reconstructed objects identified by a particle-flow algorithm [30, 31]. This algorithm combines the information from all CMS subdetectors to identify and reconstruct online individual particles emerging from the proton-proton collisions: charged hadrons, neutral hadrons, photons, muons, and electrons. These particles are then used to reconstruct jets, E_T^{miss} and hadronic τ -lepton decays, and also to quantify the isolation of leptons and photons. For the 2012 data, the electron trigger uses a 27 GeV threshold on the p_T and no other requirements on jets or E_T^{miss} are made. The combined efficiency for these triggers for $W(e\nu)H$ events to pass the offline selection criteria is $>95\%$.

For the $W(\tau\nu)H$ channel trigger, a 1-prong hadronically-decaying tau is required. The p_T of the charged track candidate coming from the tau decay is required to be above 20 GeV and the p_T of the tau (measured from all reconstructed charged and neutral decay products) above 35 GeV. Additionally, the tau is required to be isolated inside an annulus with inner radius $\Delta R = 0.2$ and outer radius $\Delta R = 0.4$, where no reconstructed charged candidates with $p_T > 1.5$ GeV must be found. A further requirement of a minimum of 70 GeV is placed on the E_T^{miss} . The efficiency of this trigger for $W(\tau\nu)H$ events that pass the offline selection criteria is $>90\%$.

The $Z(\mu\mu)H$ channel uses the same single-muon triggers as the $W(\mu\nu)H$ channel. For the $Z(ee)H$ channel, dielectron triggers with lower p_T thresholds, of 17 and 8 GeV, and tight isolation requirements are used. These triggers are nearly 100% efficient for all $Z(\ell\ell)H$ signal events that pass the final offline selection criteria.

For the $Z(\nu\nu)H$ channel, combinations of several triggers are used, all requiring E_T^{miss} to be above a given threshold. Extra requirements are added to keep the trigger rates manageable as the instantaneous luminosity increased and to reduce the E_T^{miss} thresholds in order to improve signal acceptance. A trigger with $E_T^{\text{miss}} > 150$ GeV is used for the complete data set in both 2011 and 2012. During 2011 additional triggers that require the presence of two central jets with $p_T > 20$ GeV and E_T^{miss} thresholds of 80 or 100 GeV, depending on the instantaneous luminosity, were used. During 2012 an additional trigger that required two central jets with $p_T > 30$ GeV and $E_T^{\text{miss}} > 80$ GeV was used. This last trigger was discontinued when the instantaneous luminosity exceeded $3 \times 10^{33} \text{ cm}^{-2} \text{ s}^{-1}$ and was replaced by a trigger that required $E_T^{\text{miss}} > 100$ GeV, at least two central jets with vectorial sum $p_T > 100$ GeV and individual p_T above 60 and 25 GeV, and no jet with $p_T > 40$ GeV closer than 0.5 in azimuthal angle to the E_T^{miss} direction. In order to increase signal acceptance at lower values of E_T^{miss} , triggers that require jets to be identified as coming from b quarks are used. For these triggers, two central jets with p_T above 20 or 30 GeV, depending on the luminosity conditions, are required. It is also required that at least one central jet with p_T above 20 GeV be tagged by the online combined secondary vertex (CSV) b-tagging algorithm described in Section 4. This online b-tagging requirement has an efficiency that is equivalent to that of the tight offline requirement, $\text{CSV} > 0.898$, on the value of the output of the CSV discriminant. The E_T^{miss} is required to be greater than 80 GeV for these triggers. For $Z(\nu\nu)H$ events with $E_T^{\text{miss}} > 130$ GeV, the combined trigger efficiency for $Z(\nu\nu)H$ signal events is near 100% with respect to the offline event reconstruction and selection, described in the next sections. For events with E_T^{miss} between 100 and 130 GeV the efficiency is 88%.

4 Event reconstruction

The characterization of VH events, in the channels studied here, requires the reconstruction of the following objects, all originating from a common interaction vertex: electrons, muons, taus, neutrinos, and jets (including those originating from b quarks). The charged leptons and neutrinos (reconstructed as E_T^{miss}) originate from the vector boson decays. The b-quark jets originate from the Higgs boson decays.

The reconstructed interaction vertex with the largest value of $\sum_i p_{Ti}^2$, where p_{Ti} is the transverse momentum of the i th track associated with the vertex, is selected as the primary event vertex. This vertex is used as the reference vertex for all relevant objects in the event, which are reconstructed with the particle-flow algorithm. The pileup interactions affect jet momentum reconstruction, missing transverse energy reconstruction, lepton isolation, and b-tagging efficiencies. To mitigate these effects, all charged hadrons that do not originate from the primary interaction are identified by a particle-flow-based algorithm and removed from consideration in the event. In addition, the average neutral energy density from pileup interactions is evaluated from particle-flow objects and subtracted from the reconstructed jets in the event and from the summed energy in the isolation cones used for leptons, described below [32]. These pileup-mitigation procedures are applied on an event-by-event basis.

Jets are reconstructed from particle-flow objects using the anti- k_T clustering algorithm [33], with a distance parameter of 0.5, as implemented in the FASTJET package [34, 35]. Each jet is required to lie within $|\eta| < 2.5$, to have at least two tracks associated with it, and to have electromagnetic and hadronic energy fractions of at least 1%. The last requirement removes jets originating from instrumental effects. Jet energy corrections are applied as a function of pseudorapidity and transverse momentum of the jet [36]. The missing transverse energy vector is calculated offline as the negative of the vectorial sum of transverse momenta of all particle-flow objects identified in the event, and the magnitude of this vector is referred to as E_T^{miss} in the rest of this article.

Muons are reconstructed using two algorithms [37]: one in which tracks in the silicon tracker are matched to signals in the muon detectors, and another in which a global track fit is performed, seeded by signals in the muon systems. The muon candidates used in the analysis are required to be successfully reconstructed by both algorithms. Further identification criteria are imposed on the muon candidates to reduce the fraction of tracks misidentified as muons. These include the

number of measurements in the tracker and in the muon systems, the fit quality of the global muon track and its consistency with the primary vertex. Muon candidates are considered in the $|\eta| < 2.4$ range.

Electron reconstruction requires the matching of an energy cluster in the ECAL with a track in the silicon tracker [38]. Identification criteria based on the ECAL shower shape, matching between the track and the ECAL cluster, and consistency with the primary vertex are imposed. Electron identification relies on a multivariate technique that combines observables sensitive to the amount of bremsstrahlung along the electron trajectory, the geometrical and momentum matching between the electron trajectory and associated clusters, as well as shower-shape observables. Additional requirements are imposed to remove electrons produced by photon conversions. In this analysis, electrons are considered in the pseudorapidity range $|\eta| < 2.5$, excluding the $1.44 < |\eta| < 1.57$ transition region between the ECAL barrel and endcap, where electron reconstruction is suboptimal.

Charged leptons from the W and Z boson decays are expected to be isolated from other activity in the event. For each lepton candidate, a cone is constructed around the track direction at the event vertex. The scalar sum of the transverse momentum of each reconstructed particle compatible with the primary vertex and contained within the cone is calculated, excluding the contribution from the lepton candidate itself. If this sum exceeds approximately 10% of the candidate p_T , the lepton is rejected; the exact requirement depends on the lepton η , p_T , and flavor. Including the isolation requirement, the total efficiency to reconstruct muons is in the 87–91% range, depending on p_T and η . The corresponding efficiency for electrons is in the 81–98% range.

The hadronically-decaying taus are reconstructed using the hadron plus strips (HPS) algorithm [39] which uses charged hadrons and neutral electromagnetic objects (photons) to reconstruct tau decays. Reconstructed taus are required to be in the range $|\eta| < 2.1$. In the first step of reconstruction, charged hadrons are reconstructed using the particle-flow algorithm. Since neutral pions are often produced in hadronic tau decays, the HPS algorithm is optimized to reconstruct neutral pions in the ECAL as objects called “strips”. The strip reconstruction starts by centering one strip on the most energetic electromagnetic particle and then looking for other particles in a window of 0.05 in η and 0.20 in ϕ . Strips satisfying a minimum transverse momentum of $p_T(\text{strip}) > 1 \text{ GeV}$ are combined with the charged hadrons to reconstruct the hadronic tau candidate. In the final

step of reconstruction, all charged hadrons and strips are required to be contained within a narrow cone size of $\Delta R = 2.8/p_T(\tau)$, where $p_T(\tau)$ is measured from the reconstructed hadronic tau candidate and is expressed in GeV. Further identification criteria are imposed on the tau candidate to reduce the fraction of electron and muons misidentified as taus. These include the tau candidate passing an anti-electron discriminator and an anti-muon discriminator. The isolation requirement for taus is that the sum of transverse momenta of particle-flow charged hadron and photon candidates, with $p_T > 0.5$ GeV and within a cone of $\Delta R < 0.5$, be less than 2 GeV. The tau reconstruction efficiency is approximately 50% while the misidentification rate from jets is about 1%.

Jets that originate from the hadronization of b quarks are referred to as “b jets”. The CSV b-tagging algorithm [40] is used to identify such jets. The algorithm combines the information about track impact parameters and secondary vertices within jets in a likelihood discriminant to provide separation between b jets and jets originating from light quarks, gluons, or charm quarks. The output of this CSV discriminant has values between zero and one; a jet with a CSV value above a certain threshold is referred to as being “b tagged”. The efficiency to tag b jets and the rate of misidentification of non-b jets depend on the threshold chosen, and are typically parameterized as a function of the p_T and η of the jets. These performance measurements are obtained directly from data in samples that can be enriched in b jets, such as $t\bar{t}$ and multijet events (where, for example, requiring the presence of a muon in the jets enhances the heavy-flavor content of the events). Several thresholds for the CSV output discriminant are used in this analysis. Depending on the threshold used, the efficiencies to tag jets originating from b quarks, c quarks, and light quarks or gluons are in the 50–75%, 5–25%, and 0.15–3.0% ranges, respectively.

Events from data and from the simulated samples are required to satisfy the same trigger and event reconstruction requirements. Corrections that account for the differences in the performance of these algorithms between data and simulations are computed from data and used in the analysis.

5 Event selection

The background processes to VH production with $H \rightarrow b\bar{b}$ are the production of vector bosons in association with one or more jets (V+jets), $t\bar{t}$ production, single-top-quark production, diboson production (VV), and QCD multijet production. Except for dibosons, these processes have production cross sections that are sev-

eral orders of magnitude larger than Higgs boson production. The production cross section for the VZ process, where $Z \rightarrow b\bar{b}$, is only a few times larger than the VH production cross section, and given the nearly identical final state this process provides a benchmark against which the Higgs boson search strategy can be tested.

The event selection is based on the reconstruction of the vector bosons in their leptonic decay modes and of the Higgs boson decay into two b-tagged jets. Background events are substantially reduced by requiring a significant boost of the p_T of the vector boson, $p_T(V)$, or of the Higgs boson [41]. In this kinematic region the V and H bosons recoil away from each other with a large azimuthal opening angle, $\Delta\phi(V, H)$, between them. For each channel, different $p_T(V)$ boost regions are selected. Because of different signal and background content, each $p_T(V)$ region has different sensitivity and the analysis is performed separately in each region. The results from all regions are then combined for each channel. The low-, intermediate-, and high-boost regions for the $W(\mu\nu)H$ and $W(e\nu)H$ channels are defined by $100 < p_T(V) < 130$ GeV, $130 < p_T(V) < 180$ GeV, and $p_T(V) > 180$ GeV. For the $W(\tau\nu)H$ a single $p_T(V) > 120$ GeV region is considered. For the $Z(\ell\ell)H$ channels, the low- and high-boost regions are defined by $50 < p_T(V) < 100$ GeV and $p_T(V) > 100$ GeV. For the $Z(\nu\nu)H$ channel E_T^{miss} is used to define the low-, intermediate-, and high-boost $p_T(V)$ regions as $100 < E_T^{\text{miss}} < 130$ GeV, $130 < E_T^{\text{miss}} < 170$ GeV, and $E_T^{\text{miss}} > 170$ GeV, respectively. In the rest of the article the term “boost region” is used to refer to these $p_T(V)$ regions.

Candidate $W \rightarrow \ell\nu$ decays are identified by requiring the presence of a single-isolated lepton and additional missing transverse energy. Muons are required to have $p_T > 20$ GeV; the corresponding thresholds for electrons and taus are 30 and 40 GeV, respectively. For the $W(\ell\nu)H$ and $W(\tau\nu)H$ channels, E_T^{miss} is required to be >45 and >80 GeV, respectively, to reduce contamination from QCD multijet processes. To further reduce this contamination, it is also required for the $W(\ell\nu)H$ channels that the azimuthal angle between the E_T^{miss} direction and the lepton be $< \pi/2$, and that the lepton isolation for the low-boost region be tighter.

Candidate $Z \rightarrow \ell\ell$ decays are reconstructed by combining isolated, oppositely-charged pairs of electrons or muons and requiring the dilepton invariant mass to satisfy $75 < m_{\ell\ell} < 105$ GeV. The p_T for each lepton is required to be >20 GeV.

The identification of $Z \rightarrow \nu\bar{\nu}$ decays requires the E_T^{miss} in the event to be within the boost regions described above. The QCD multijet background is reduced to

negligible levels in this channel when requiring that the E_T^{miss} does not originate from mismeasured jets. To that end three event requirements are made. First, for the high-boost region, a $\Delta\phi(E_T^{\text{miss}}, \text{jet}) > 0.5$ radians requirement is applied on the azimuthal angle between the E_T^{miss} direction and the closest jet with $|\eta| < 2.5$ and $p_T > 20$ GeV for the 7 TeV analysis or $p_T > 25$ GeV for the 8 TeV analysis (where more pileup interactions are present). For the low- and intermediate-boost regions the requirement is tightened to $\Delta\phi(E_T^{\text{miss}}, \text{jet}) > 0.7$ radians. The second requirement is that the azimuthal angle between the missing transverse energy direction as calculated from charged tracks only (with $p_T > 0.5$ GeV and $|\eta| < 2.5$) and the E_T^{miss} direction, $\Delta\phi(E_T^{\text{miss}}, E_T^{\text{miss}}(\text{tracks}))$, should be smaller than 0.5 radians. The third requirement is made for the low-boost region where the E_T^{miss} significance (defined as the ratio between the E_T^{miss} and the square root of the total transverse energy in the calorimeter, measured in GeV) should be larger than 3. To reduce background events from $t\bar{t}$ and WZ production in the $W(\ell\nu)H$, $W(\tau\nu)H$, and $Z(\nu\nu)H$ channels, events with an additional number of isolated leptons, $N_{a\ell} > 0$, with $p_T > 20$ GeV are rejected.

The reconstruction of the $H \rightarrow b\bar{b}$ decay proceeds by selecting the pair of jets in the event, each with $|\eta| < 2.5$ and p_T above a minimum threshold, for which the value of the magnitude of the vectorial sum of their transverse momenta, $p_T(jj)$, is the highest. These jets are then also required to be tagged by the CSV algorithm, with the value of the CSV discriminator above a minimum threshold. The background from V+jets and diboson production is reduced significantly when the b-tagging requirements are applied and processes where the two jets originate from genuine b quarks dominate the final selected data sample.

After all event selection criteria described in this section are applied, the dijet invariant-mass resolution of the two b jets from the Higgs decay is approximately 10%, depending on the p_T of the reconstructed Higgs boson, with a few percent shift on the value of the mass peak. The Higgs boson mass resolution is further improved by applying multivariate regression techniques similar to those used at the CDF experiment [42]. An additional correction, beyond the standard CMS jet energy corrections, is computed for individual b jets in an attempt to recalibrate to the true b-quark energy. For this purpose, a specialized BDT is trained on simulated $H \rightarrow b\bar{b}$ signal events with inputs that include detailed jet structure information which differs in jets from b quarks from that of jets from light-flavor quarks or gluons. These inputs include variables related to several properties of the secondary vertex (when reconstructed), information about tracks, jet constituents, and other variables related to the energy reconstruction of the jet. Be-

cause of semileptonic b-hadron decays, jets from b quarks contain, on average, more leptons and a larger fraction of missing energy than jets from light quarks or gluons. Therefore, in the cases where a low- p_T lepton is found in the jet or in its vicinity, the following variables are also included in the BDT regression: the p_T of the lepton, the ΔR distance between the lepton and the jet directions, and the transverse momentum of the lepton relative to the jet direction. For the $Z(\ell\ell)H$ channels the E_T^{miss} in the event and the azimuthal angle between the E_T^{miss} and each jet are also considered in the regression. The output of the BDT regression is the corrected jet energy. The average improvement on the mass resolution, measured on simulated signal samples, when the corrected jet energies are used is $\approx 15\%$, resulting in an increase in the analysis sensitivity of 10–20%, depending on the specific channel. This improvement is shown in Fig. 1 for simulated samples of $Z(\ell\ell)H(bb)$ events where the improvement in resolution is $\approx 25\%$. The validation of the regression technique in data is done with samples of $Z \rightarrow \ell\ell$ events with two b-tagged jets and in $t\bar{t}$ -enriched samples in the lepton+jets final state. In the $Z \rightarrow \ell\ell$ case, when the jets are corrected by the regression procedure, the p_T balance distribution, between the Z boson, reconstructed from the leptons, and the b-tagged dijet system is improved to be better centered at zero and narrower than when the regression correction is not applied. In the $t\bar{t}$ -enriched case, the reconstructed top-quark mass distribution is closer to the nominal top-quark mass and also narrower than when the correction is not applied. In both cases the distributions for data and the simulated samples are in very good agreement after the regression correction is applied.

The signal region is defined by events that satisfy the vector boson and Higgs boson reconstruction criteria described above together with the requirements listed in Table 1. In the final stage of the analysis, to better separate signal from background under different Higgs boson mass hypotheses, an event BDT discriminant is trained separately at each mass value using simulated samples for signal and all background processes. The training of this BDT is performed with all events in the signal region. The set of event input variables used, listed in Table 2, is chosen by iterative optimization from a larger number of potentially discriminating variables. Among the most discriminant variables for all channels are the dijet invariant mass distribution ($m(jj)$), the number of additional jets (N_{aj}), the value of CSV for the Higgs boson daughter with the second largest CSV value (CSV_{min}), and the distance between Higgs boson daughters ($\Delta R(jj)$). It has been suggested that variables related to techniques that study in more detail the sub-structure of jets could help improve the sensitivity of the $H \rightarrow b\bar{b}$ searches [41].

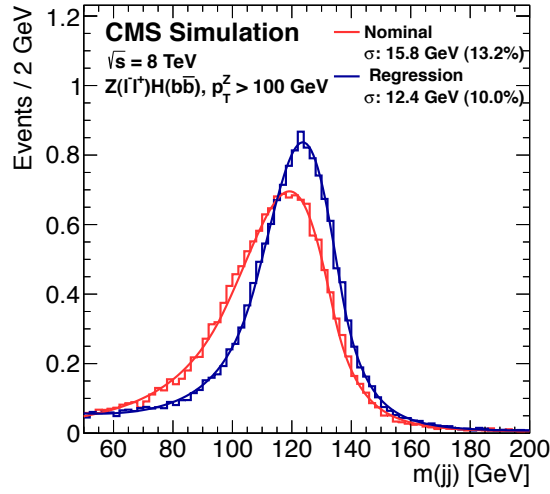


Figure 1: Dijet invariant mass distribution for simulated samples of $Z(\ell\ell)H(bb)$ events ($m_H = 125$ GeV), before (red) and after (blue) the energy correction from the regression procedure is applied. A Bukin function [43] is fit to the distribution and the fitted width of the core of the distribution is displayed on the figure.

In this analysis, several combinations of such variables were considered as additional inputs to the BDT discriminant. However they did not yield significant gains in sensitivity and are not included in the final training used.

A fit is performed to the shape of the output distribution of the event BDT discriminant to search for events resulting from Higgs boson production. Before testing all events through this final discriminant, events are classified based on where they fall in the output distributions of several other background-specific BDT discriminants that are trained to discern signal from individual background processes. This technique, similar to the one used by the CDF collaboration [44], divides the samples into four distinct subsets that are enriched in $t\bar{t}$, V+jets, dibosons, and VH. The increase in the analysis sensitivity from using this technique in the $Z(\nu\nu)H$ and $W(\ell\nu)H$ channels is 5–10%. For the $Z(\ell\ell)H$ channel the improvement is not as large and therefore the technique is not used for that case. The technique is also not used in the $W(\tau\nu)H$ channel because of the limited size of the simulated event samples available for training multiple BDT discriminants. The first background-specific BDT discriminant is trained to separate $t\bar{t}$ from VH, the second one is trained to separate V+jets from VH, and the third one separates diboson events from VH. The output distributions of the background-specific BDTs are used to separate events in four subsets: those that fail a requirement

Table 1: Selection criteria that define the signal region. Entries marked with “–” indicate that the variable is not used in the given channel. If different, the entries in square brackets indicate the selection for the different boost regions as defined in the first row of the table. The p_T thresholds for the highest and second highest p_T jets are $p_T(j_1)$ and $p_T(j_2)$, respectively. The transverse momentum of the leading tau track is $p_T(\text{track})$. The values listed for kinematic variables are in units of GeV, and for angles in units of radians.

Variable	W($\ell\nu$)H			W($\tau\nu$)H	Z($\ell\ell$)H		Z($\nu\nu$)H		
$p_T(V)$	[100–130]	[130–180]	[>180]	[>120]	[50–100]	[>100]	[100–130]	[130–170]	[>170]
$m_{\ell\ell}$	–	–	–	–	[75–105]		–	–	–
$p_T(j_1)$	>30	>30	>30	>30	>20		>60		
$p_T(j_2)$	>30	>30	>30	>30	>20		>30		
$p_T(jj)$	>100	>120	>120	>120	–		[>100]	[>130]	[>130]
$m(jj)$	<250	<250	<250	<250	[40–250] [< 250]		<250		
E_T^{miss}	>45	>80	>80	>80	–		[100–130]	[130–170]	[> 170]
$p_T(\tau)$	–	–	–	>40	–		–		
$p_T(\text{track})$	–	–	–	>20	–		–		
CSV _{max}	>0.40	>0.40	>0.40	>0.40	[>0.50] [>0.244]		>0.679		
CSV _{min}	>0.40	>0.40	>0.40	>0.40	>0.244		>0.244		
N_{aj}	–	–	–	–	–		[< 2] [–] [–]		
N_{al}	=0	=0	=0	=0	–		=0		
$\Delta\phi(V, H)$	–	–	–	–	–		>2.0		
$\Delta\phi(E_T^{\text{miss}}, \text{jet})$	–	–	–	–	–		[>0.7] [>0.7] [>0.5]		
$\Delta\phi(E_T^{\text{miss}}, E_T^{\text{miss}}(\text{tracks}))$	–	–	–	–	–		<0.5		
E_T^{miss} significance	–	–	–	–	–		[>3] [–] [–]		
$\Delta\phi(E_T^{\text{miss}}, \ell)$	< $\pi/2$	< $\pi/2$	< $\pi/2$	< $\pi/2$	–		–		

on the $t\bar{t}$ BDT are classified as $t\bar{t}$ -like events, those that pass the $t\bar{t}$ BDT requirement but fail a requirement on the V+jets BDT are classified as V+jets-like events, those that pass the V+jets BDT requirement but fail the requirement on the diboson BDT are classified as diboson-like events and, finally, those that pass all BDT requirements are considered VH-enriched events. The events in each subset are then run through the final event BDT discriminant and the resulting distribution, now composed of four distinct subsets of events, is used as input to the fitting procedure.

As a validation of the multivariate approach to this analysis, these BDT discriminants are also trained to find diboson signals (ZZ and WZ, with $Z \rightarrow b\bar{b}$) rather than the VH signal. The event selection used in this case is identical to that used for the VH search.

As a cross-check to the BDT-based analysis, a simpler analysis is done by performing a fit to the shape of the dijet invariant mass distribution of the two jets associated with the reconstructed Higgs boson, $m(jj)$. The event selection for this

Table 2: Variables used in the training of the event BDT discriminant. Jets are counted as additional jets if they satisfy the following: $p_T > 20 \text{ GeV}$ and $|\eta| < 4.5$ for $W(\ell\nu)H$, $p_T > 20 \text{ GeV}$ and $|\eta| < 2.5$ for $Z(\ell\ell)H$, and $p_T > 25 \text{ GeV}$ and $|\eta| < 4.5$ for $Z(\nu\nu)H$.

Variable
$p_T(j_1), p_T(j_2)$: transverse momentum of each Higgs boson daughter
$m(jj)$: dijet invariant mass
$p_T(jj)$: dijet transverse momentum
$p_T(V)$: vector boson transverse momentum (or E_T^{miss})
N_{aj} : number of additional jets (see caption)
CSV_{max} : value of CSV for the Higgs boson daughter with largest CSV value
CSV_{min} : value of CSV for the Higgs boson daughter with second largest CSV value
$\Delta\phi(V, H)$: azimuthal angle between V (or E_T^{miss}) and dijet
$ \Delta\eta(jj) $: difference in η between Higgs boson daughters
$\Delta R(jj)$: distance in η - ϕ between Higgs boson daughters
$\Delta\theta_{\text{pull}}$: color pull angle [45]
$\Delta\phi(E_T^{\text{miss}}, \text{jet})$: azimuthal angle between E_T^{miss} and the closest jet (only for $Z(\nu\nu)H$)
maxCSV_{aj} : maximum CSV of the additional jets in an event (only for $Z(\nu\nu)H$ and $W(\ell\nu)H$)
$\text{min}\Delta R(H, aj)$: minimum distance between an additional jet and the Higgs boson candidate (only for $Z(\nu\nu)H$ and $W(\ell\nu)H$)
Invariant mass of the VH system (only for $Z(\ell\ell)H$)
Cosine of the angle between the direction of the V boson in the rest frame of the VH system and the direction of the VH system in the laboratory frame (only for $Z(\ell\ell)H$)
Cosine of the angle between the direction of one of the leptons in the rest frame of the Z boson and the direction of the Z boson in the laboratory frame (only for $Z(\ell\ell)H$)
Cosine of the angle between the direction of one of the jets in the rest frame of the reconstructed Higgs boson and the direction of the reconstructed Higgs boson in the laboratory frame (only for $Z(\ell\ell)H$)

analysis is more restrictive than the one used in the BDT analysis and is optimized for sensitivity in this single variable. Table 3 lists the event selection of the $m(jj)$ analysis. Since the diboson background also exhibits a peak in the $m(jj)$ distribution from Z bosons that decay into b quark pairs, the distribution is also used to measure the consistency of the diboson rate with the expectation from the standard model. A consistent rate measurement would support the validity of the estimate of the background processes in the Higgs boson search.

6 Background control regions

Appropriate control regions are identified in data and used to validate the simulation modeling of the distributions used as input to the BDT discriminants, and to obtain scale factors used to adjust the simulation event yield estimates for the most important background processes: production of W and Z bosons in association with jets and $t\bar{t}$ production. For the W and Z backgrounds the control regions are defined such that they are enriched in either heavy-flavor (HF) or light-flavor (LF) jets. Furthermore, these processes are split according to how many of the two jets selected in the Higgs boson reconstruction originate from b quarks, and

Table 3: Selection criteria for the samples used in the $m(\text{jj})$ analysis in each channel. Entries marked with “–” indicate that the variable is not used in the given channel. If different, the entries in square brackets indicate the selection for the different boost regions as defined in the first row of the table. The p_{T} thresholds for the highest and second highest p_{T} jets are $p_{\text{T}}(\text{j}_1)$ and $p_{\text{T}}(\text{j}_2)$, respectively. The transverse momentum of the leading tau track is $p_{\text{T}}(\text{track})$. The values listed for kinematic variables are in units of GeV, and for angles in units of radians.

Variable	W($\ell\nu$)H	W($\tau\nu$)H	Z($\ell\ell$)H	Z($\nu\nu$)H
$p_{\text{T}}(\text{V})$	[100–150] [>150] (e) [100–130] [130–180] [>180] (μ)	[<250]	[50–100] [100–150] [>150]	[100–130] [130–170] [>170]
$m_{\ell\ell}$	–	–	$75 < m_{\ell\ell} < 105$	–
$p_{\text{T}}(\text{j}_1)$	>30	>30	>20	[>60][>60][>80]
$p_{\text{T}}(\text{j}_2)$	>30	>30	>20	>30
$p_{\text{T}}(\text{jj})$	>100	>120	–	[>110][>140][>190]
N_{aj}	$=0$	$=0$	–	$=0$
$N_{\text{a}\ell}$	$=0$	$=0$	–	$=0$
$E_{\text{T}}^{\text{miss}}$	>45	>80	<60	–
$p_{\text{T}}(\tau)$	–	>40	–	–
$p_{\text{T}}(\text{track})$	–	>20	–	–
CSV _{max}	0.898	0.898	0.679	0.898
CSV _{min}	>0.5	>0.4	>0.5	>0.5
$\Delta\phi(\text{V}, \text{H})$	>2.95	>2.95	–	>2.95
$\Delta R(\text{jj})$	–	–	[–][–][<1.6]	–
$\Delta\phi(E_{\text{T}}^{\text{miss}}, \text{jet})$	–	–	–	[>0.7][>0.7][>0.5]
$\Delta\phi(E_{\text{T}}^{\text{miss}}, E_{\text{T}}^{\text{miss}}(\text{tracks}))$	–	–	–	<0.5
$\Delta\phi(E_{\text{T}}^{\text{miss}}, \ell)$	$<\pi/2$	–	–	–

separate scale factors are obtained for each case. The notation used is: $V + \text{udscg}$ for the case where none of the jets originate from a b quark, $V + b$ for the case where only one of the jets is from a b quark, and $V + b\bar{b}$ for the case where both jets originate from b quarks.

To obtain the scale factors by which the simulated event yields are adjusted, a set of binned likelihood fits is simultaneously performed to CSV distributions of jets for events in the control regions. These fits are done separately for each channel. Several other distributions are also fit to verify consistency. These scale factors account not only for cross section discrepancies, but also for potential residual differences in physics object selection. Therefore, separate scale factors are used for each background process in the different channels. The uncertainties in the scale factor determination include two components: the statistical uncertainty due to the finite size of the samples and the systematic uncertainty. The latter is obtained by subtracting, in quadrature, the statistical component from the full uncertainty which includes the effect of various sources of systematic uncertainty such as b -tagging, jet energy scale, and jet energy resolution.

Tables 4–6 list the selection criteria used to define the control regions for the $W(\ell\nu)H$, $Z(\ell\ell)H$, and $Z(\nu\nu)H$ channels, respectively. Because of the limited size of the simulated event samples the scale factors obtained for the $W(\ell\nu)H$ channels are applied to the $W(\tau\nu)H$ channel. Table 7 summarizes the fit results for all channels for the 8 TeV data. The scale factors are found to be close to unity for all processes except for $V + b$ for which the scale factors are consistently found to be close to two. In this case, most of the excess occurs in the region of low CSV_{\min} values in which events with two displaced vertices are found relatively close to each other, within a distance $\Delta R < 0.5$ defined by the directions of their displacement trajectories with respect to the primary vertex. This discrepancy is interpreted as arising mainly from mismodeling in the generator parton shower of the process of gluon-splitting to b -quark pairs. In this process the dominant contribution typically contains a low- p_T b quark that can end up not being reconstructed as a jet above the p_T threshold used in the analysis, or that is merged with the jet from the more energetic b quark. These discrepancies are consistent with similar observations in other studies of the production of vector bosons in association with heavy-flavor quarks by the ATLAS and CMS experiments [46–48].

Figures 2 and 3 show examples of distributions for variables in the simulated samples and in data for different control regions and for different channels. The

Table 4: Definition of the control regions for the $W(\mu\nu)H$ and the $W(e\nu)H$ channels. The same selection is used for all boost regions. Here, LF and HF refer to light- and heavy-flavor jets. The values listed for kinematic variables are in units of GeV. Because of the limited size of the simulated samples the scale factors derived in these control regions are also applied to the $W(\tau\nu)H$ channel.

Variable	W+LF	$t\bar{t}$	W+HF
$p_T(j_1)$	>30	>30	>30
$p_T(j_2)$	>30	>30	>30
$p_T(jj)$	>100	>100	>100
$m(jj)$	<250	<250	$<250, \notin [90-150]$
CSV_{\max}	$\in [0.244-0.898]$	>0.898	>0.898
N_{aj}	<2	>1	$=0$
$N_{a\ell}$	$=0$	$=0$	$=0$
E_T^{miss}	>45	>45	>45
E_T^{miss} significance	$>2.0(\mu) >3.0(e)$	–	–

Table 5: Definition of the control regions for the $Z(\ell\ell)H$ channel. The same selection is used for both the low- and high-boost regions. The values listed for kinematic variables are in units of GeV.

Variable	Z+jets	$t\bar{t}$
$m_{\ell\ell}$	$[75-105]$	$\notin [75-105]$
$p_T(j_1)$	>20	>20
$p_T(j_2)$	>20	>20
$p_T(V)$	>50	$[50-100]$
$m(jj)$	$<250, \notin [80-150]$	$<250, \notin [80-150]$
CSV_{\max}	>0.244	>0.244
CSV_{\min}	>0.244	>0.244

scale factors described above have been applied to the corresponding simulated samples.

7 Uncertainties

The systematic uncertainties that affect the results presented in this article are listed in Table 8 and are described in more detail below.

The uncertainty in the CMS luminosity measurement is estimated to be 2.2% for the 2011 data [49] and 2.6% for the 2012 data [50]. Muon and electron trigger, re-

Table 6: Definition of the control regions for the $Z(\nu\nu)H$ channel. If different, the entries in square brackets indicate the selection for the different boost regions as defined by the E_T^{miss} in the first row of the table. The values listed for kinematic variables are in units of GeV, and for angles in units of radians.

Variable	Z+LF	Z+HF	$t\bar{t}$	W+LF	W+HF
E_T^{miss}	[100–130] [130–170] [>170]	[100–130] [130–170] [>170]	[100–130] [130–170] [>170]	[100–130] [130–170] [>170]	[100–130] [130–170] [>170]
$p_T(j_1)$	>60	>60	>60	>60	>60
$p_T(j_2)$	>30	>30	>30	>30	>30
$p_T(j)$	[>100] [>130] [>130]	[>100] [>130] [>130]	[>100] [>130] [>130]	[>100] [>130] [>130]	[>100] [>130] [>130]
$m(j)$	<250	<250 , $\notin[100-140]$	<250 , $\notin[100-140]$	<250	<250 , $\notin[100-140]$
CSV _{max}	[0.244 – 0.898]	>0.679	>0.898	[0.244 – 0.898]	>0.679
CSV _{min}	–	>0.244	–	–	>0.244
N_{aj}	[<2] [–] [–]	[<2] [–] [–]	≥ 1	=0	=0
N_{af}	=0	=0	=1	=1	=1
$\Delta\phi(V, H)$	–	>2.0	–	–	>2.0
$\Delta\phi(E_T^{\text{miss}}, \text{jet})$	[>0.7] [>0.7] [>0.5]	[>0.7] [>0.7] [>0.5]	[>0.7] [>0.7] [>0.5]	[>0.7] [>0.7] [>0.5]	[>0.7] [>0.7] [>0.5]
$\Delta\phi(E_T^{\text{miss}}, E_T^{\text{miss}}(\text{tracks}))$	<0.5	<0.5	–	–	–
E_T^{miss} significance	[>3] [–] [–]	[>3] [–] [–]	[>3] [–] [–]	[>3] [–] [–]	[>3] [–] [–]

construction, and identification efficiencies are determined in data from samples of leptonic Z-boson decays. The uncertainty on the event yields resulting from the trigger efficiency estimate is 2% per lepton and the uncertainty on the identification efficiency is also 2% per lepton. The parameters describing the $Z(\nu\nu)H$ trigger efficiency turn-on curve have been varied within their statistical uncertainties and also estimated for different assumptions on the methods used to derive the efficiency. This results in an event yield uncertainty of about 3%.

The jet energy scale is varied within its uncertainty as a function of jet p_T and η . The efficiency of the analysis selection is recomputed to assess the variation in event yields. Depending on the process, a 2–3% yield variation is found. The effect of the uncertainty on the jet energy resolution is evaluated by smearing the jet energies according to the measured uncertainty. Depending on the process, a 3–6% variation in event yields is obtained. The uncertainties in the jet energy scale and resolution also have an effect on the shape of the BDT output distribution. The impact of the jet energy scale uncertainty is determined by recomputing the BDT output distribution after shifting the energy scale up and down by its uncertainty. Similarly, the impact of the jet energy resolution is determined by recomputing the BDT output distribution after increasing or decreasing the jet energy resolution. An uncertainty of 3% is assigned to the event yields of all processes in the $W(\ell\nu)H$ and $Z(\nu\nu)H$ channels due to the uncertainty related to the missing transverse energy estimate.

Data/MC b-tagging scale factors are measured in heavy-flavor enhanced samples of jets that contain muons and are applied consistently to jets in signal and background events. The measured uncertainties for the b-tagging scale factors are: 3% per b-quark tag, 6% per charm-quark tag, and 15% per mistagged jet (originating from gluons and light u, d, or s quarks) [40]. These translate into yield uncer-

Table 7: Data/MC scale factors for 8 TeV data derived from the control regions, where the first quoted uncertainty is statistical and the second is systematic. The muon and electron channels in $Z(\ell\ell)H$ and $W(\ell\nu)H$ are simultaneously fit to determine average scale factors. For the $Z(\ell\ell)H$ channel only four scale factors are derived, valid for both the low and high $p_T(V)$ boost regions. Because of the limited size of the simulated event samples the scale factors obtained for the $W(\ell\nu)H$ channels are also applied to the $W(\tau\nu)H$ channel.

Process	$W(\ell\nu)H$	$Z(\ell\ell)H$	$Z(\nu\nu)H$
Low $p_T(V)$			
$W + \text{udscg}$	$1.03 \pm 0.01 \pm 0.05$	–	$0.83 \pm 0.02 \pm 0.04$
$W + b$	$2.22 \pm 0.25 \pm 0.20$	–	$2.30 \pm 0.21 \pm 0.11$
$W + b\bar{b}$	$1.58 \pm 0.26 \pm 0.24$	–	$0.85 \pm 0.24 \pm 0.14$
$Z + \text{udscg}$	–	$1.11 \pm 0.04 \pm 0.06$	$1.24 \pm 0.03 \pm 0.09$
$Z + b$	–	$1.59 \pm 0.07 \pm 0.08$	$2.06 \pm 0.06 \pm 0.09$
$Z + b\bar{b}$	–	$0.98 \pm 0.10 \pm 0.08$	$1.25 \pm 0.05 \pm 0.11$
$t\bar{t}$	$1.03 \pm 0.01 \pm 0.04$	$1.10 \pm 0.05 \pm 0.06$	$1.01 \pm 0.02 \pm 0.04$
Intermediate $p_T(V)$			
$W + \text{udscg}$	$1.02 \pm 0.01 \pm 0.07$	–	$0.93 \pm 0.02 \pm 0.04$
$W + b$	$2.90 \pm 0.26 \pm 0.20$	–	$2.08 \pm 0.20 \pm 0.12$
$W + b\bar{b}$	$1.30 \pm 0.23 \pm 0.14$	–	$0.75 \pm 0.26 \pm 0.11$
$Z + \text{udscg}$	–	–	$1.19 \pm 0.03 \pm 0.07$
$Z + b$	–	–	$2.30 \pm 0.07 \pm 0.08$
$Z + b\bar{b}$	–	–	$1.11 \pm 0.06 \pm 0.12$
$t\bar{t}$	$1.02 \pm 0.01 \pm 0.15$	–	$0.99 \pm 0.02 \pm 0.03$
High $p_T(V)$			
$W + \text{udscg}$	$1.04 \pm 0.01 \pm 0.07$	–	$0.93 \pm 0.02 \pm 0.03$
$W + b$	$2.46 \pm 0.33 \pm 0.22$	–	$2.12 \pm 0.22 \pm 0.10$
$W + b\bar{b}$	$0.77 \pm 0.25 \pm 0.08$	–	$0.71 \pm 0.25 \pm 0.15$
$Z + \text{udscg}$	–	$1.11 \pm 0.04 \pm 0.06$	$1.17 \pm 0.02 \pm 0.08$
$Z + b$	–	$1.59 \pm 0.07 \pm 0.08$	$2.13 \pm 0.05 \pm 0.07$
$Z + b\bar{b}$	–	$0.98 \pm 0.10 \pm 0.08$	$1.12 \pm 0.04 \pm 0.10$
$t\bar{t}$	$1.00 \pm 0.01 \pm 0.11$	$1.10 \pm 0.05 \pm 0.06$	$0.99 \pm 0.02 \pm 0.03$

tainties in the 3–15% range, depending on the channel and the specific process. The shape of the BDT output distribution is also affected by the shape of the CSV distributions and an uncertainty is assigned according to a range of variations of the CSV distributions.

The total VH signal cross section has been calculated to NNLO accuracy, and the total theoretical uncertainty is $\approx 4\%$ [51], including the effect of scale variations and PDF uncertainties [25, 52–55]. This analysis is performed in the boosted regime, and differences in the p_T spectrum of the V and H bosons between data and MC introduce systematic effects in the signal acceptance and efficiency estimates. Two calculations are available that evaluate the NLO electroweak (EW) [56–58] and NNLO QCD [59] corrections to VH production in the boosted regime. Both the electroweak and QCD corrections are applied to the signal samples. The estimated uncertainties of the NLO electroweak corrections are 2% for both the ZH and WH production processes. The estimate for the NNLO QCD correction results in an uncertainty of 5% for both the ZH and WH production processes.

The uncertainty in the background event yields estimated from data is approximately 10%. For V+jets, the difference between the shape of the BDT output distribution for events generated with the MADGRAPH and the HERWIG ++ Monte Carlo generators is considered as a shape systematic uncertainty. For $t\bar{t}$ the differences in the shape of the BDT output distribution between the one obtained from the nominal MADGRAPH samples and those obtained from the POWHEG and MC@NLO [60] generators are considered as shape systematic uncertainties.

An uncertainty of 15% is assigned to the event yields obtained from simulation for single-top-quark production. For the diboson backgrounds, a 15% cross section uncertainty is assumed. These uncertainties are consistent with the CMS measurements of these processes [61, 62]. The limited number of MC simulated events is also taken into account as a source of uncertainty.

The combined effect of the systematic uncertainties results in an increase of about 15% on the expected upper limit on the Higgs boson production cross section and in a reduction of 15% on the expected significance of an observation when the Higgs boson is present in the data at the predicted standard model rate.

Table 8: Information about each source of systematic uncertainty, including whether it affects the shape or normalization of the BDT output, the uncertainty in signal or background event yields, and the relative contribution to the expected uncertainty in the signal strength, μ (defined as the ratio of the best-fit value for the production cross section for a 125 GeV Higgs boson, relative to the standard model cross section). Due to correlations, the total systematic uncertainty is less than the sum in quadrature of the individual uncertainties. The last column shows the percentage decrease in the total signal strength uncertainty, including statistical, when removing that specific source of uncertainty. The ranges quoted are due to the difference between 7 and 8 TeV data, different channels, specific background processes, and the different Higgs boson mass hypotheses. See text for details.

Source	Type	Event yield uncertainty range (%)	Individual contribution to μ uncertainty (%)	Effect of removal on μ uncertainty (%)
Luminosity	norm.	2.2–2.6	<2	<0.1
Lepton efficiency and trigger (per lepton)	norm.	3	<2	<0.1
$Z(\nu\nu)H$ triggers	shape	3	<2	<0.1
Jet energy scale	shape	2–3	5.0	0.5
Jet energy resolution	shape	3–6	5.9	0.7
Missing transverse energy	shape	3	3.2	0.2
b-tagging	shape	3–15	10.2	2.1
Signal cross section (scale and PDF)	norm.	4	3.9	0.3
Signal cross section (p_T boost, EW/QCD)	norm.	2/5	3.9	0.3
Monte Carlo statistics	shape	1–5	13.3	3.6
Backgrounds (data estimate)	norm.	10	15.9	5.2
Single-top-quark (simulation estimate)	norm.	15	5.0	0.5
Dibosons (simulation estimate)	norm.	15	5.0	0.5
MC modeling (V+jets and tt)	shape	10	7.4	1.1

8 Results

Results are obtained from combined signal and background binned likelihood fits to the shape of the output distribution of the BDT discriminants. These are trained separately for each channel and for each Higgs boson mass hypothesis in the 110–135 GeV range. In the simultaneous fit to all channels, in all boost regions, the BDT shape and normalization for signal and for each background component are allowed to vary within the systematic and statistical uncertainties described in Section 7. These uncertainties are treated as independent nuisance parameters in the fit. All nuisance parameters, including the scale factors described in Section 6, are adjusted by the fit.

In total 14 BDT distributions are considered. Figure 4 shows an example of these distributions after the fit for the high-boost region of the $Z(\nu\nu)H$ channel, for the $m_H = 125$ GeV mass hypothesis. The four partitions in the left panel correspond to the subsets enriched in $t\bar{t}$, V +jets, diboson, and VH production, as described in Section 5. The right panel shows the right-most, VH -enriched, partition in more detail. For completeness, all 14 BDT distributions used in the fit are shown in Figs. 10–14 in Appendix A. Table 9 lists, for partial combinations of channels, the total number of events in the four highest bins of their corresponding BDT for the expected backgrounds, for the 125 GeV SM Higgs boson signal, and for data. An excess compatible with the presence of the SM Higgs boson is observed. Figure 5 combines the BDT outputs of all channels where the events are gathered in bins of similar expected signal-to-background ratio, as given by the value of the output of their corresponding BDT discriminant (trained with a Higgs boson mass hypothesis of 125 GeV). The observed excess of events in the bins with the largest signal-to-background ratio is consistent with what is expected from the production of the standard model Higgs boson.

The results of all channels, for all boost regions and for the 7 and 8 TeV data, are combined to obtain 95% confidence level (CL) upper limits on the product of the VH production cross section times the $H \rightarrow b\bar{b}$ branching fraction, with respect to the expectations for a standard model Higgs boson (σ/σ_{SM}). At each mass point the observed limit, the median expected limit, and the 1 and 2 standard deviation bands are calculated using the modified frequentist method CL_s [63–65]. Figure 6 displays the results.

For a Higgs boson mass of 125 GeV the expected limit is 0.95 and the observed limit is 1.89. Given that the resolution for the reconstructed Higgs boson mass is $\approx 10\%$, these results are compatible with a Higgs mass of 125 GeV. This is demon-

Table 9: The total number of events for partial combinations of channels in the four highest bins of their corresponding BDT for the expected backgrounds (B), for the 125 GeV SM Higgs boson VH signal (S), and for data. Also shown is the signal-to-background ratio (S/B).

	W($\ell\nu$)H			W($\tau\nu$)H		Z($\ell\ell$)H		Z($\nu\nu$)H	
Process	Low p_T (V)	Int. p_T (V)	High p_T (V)		Low p_T (V)	High p_T (V)	Low p_T (V)	Int. p_T (V)	High p_T (V)
V + bb	25.2	22.4	15.9	4.3	158.6	36.2	177.3	98.3	68.2
V + b	3.1	2.9	9.6	1.2	95.8	14.6	84.7	58.3	27.6
V + udscg	4.5	8.5	10.0	2.5	62.3	8.7	57.6	31.0	21.6
t \bar{t}	113.2	106.5	50.3	22.6	107.0	6.9	153.8	87.4	39.2
Single-top-quark	24.1	20.3	14.7	7.4	2.9	0.4	54.5	20.1	11.7
VV(udscg)	0.3	1.3	1.2	0.2	2.4	0.4	2.3	1.5	1.4
VZ(bb)	1.1	1.4	2.3	1.1	11.0	2.7	9.5	6.9	7.7
Total backgrounds	171.7	163.4	104.1	39.4	439.8	69.8	539.7	303.5	177.4
VH	3.0	6.0	8.3	1.4	5.5	6.3	8.5	8.5	11.5
Data	185	182	128	35	425	77	529	322	188
S/B (%)	1.7	3.7	8.0	3.4	1.3	9.0	1.6	2.8	6.5

strated by the red dashed line in the left panel of Fig. 6, which is the expected limit obtained from the sum of expected background and the signal of a SM Higgs boson with a mass of 125 GeV.

For all channels an excess of events over the expected background contributions is indicated by the fits of the BDT output distributions. The probability (p-value) to observe data as discrepant as observed under the background-only hypothesis is shown in the right panel of Fig. 6 as a function of the assumed Higgs boson mass. For $m_H = 125$ GeV, the excess of observed events corresponds to a local significance of 2.1 standard deviations away from the background-only hypothesis. This is consistent with the 2.1 standard deviations expected when assuming the standard model prediction for Higgs boson production.

The relative sensitivity of the channels that are topologically distinct is demonstrated in Table 10 for $m_H = 125$ GeV. The table lists the expected and observed limits and local significance for the W($\ell\nu$)H and W($\tau\nu$)H channels combined, for the Z($\ell\ell$)H channels combined, and for the Z($\nu\nu$)H channel.

The best-fit values of the production cross section for a 125 GeV Higgs boson, relative to the standard model cross section (signal strength, μ), are shown in the left panel of Fig. 7 for the W($\ell\nu$)H and W($\tau\nu$)H channels combined, for the Z($\ell\ell$)H channels combined, and for the Z($\nu\nu$)H channel. The observed signal strengths are consistent with each other, and the value for the signal strength for the combination of all channels is 1.0 ± 0.5 . In the right panel of Fig. 7 the correlation

Table 10: The expected and observed 95% CL upper limits on the product of the VH production cross section times the $H \rightarrow b\bar{b}$ branching fraction, with respect to the expectations for the standard model Higgs boson, for partial combinations of channels and for all channels combined, for $m_H = 125$ GeV. Also shown are the expected and observed local significances.

$m_H = 125$ GeV	$\sigma/\sigma_{\text{SM}}$ (95% CL) median expected	$\sigma/\sigma_{\text{SM}}$ (95% CL) observed	Significance expected	Significance observed
$W(\ell\nu, \tau\nu)H$	1.6	2.3	1.3	1.4
$Z(\ell\ell)H$	1.9	2.8	1.1	0.8
$Z(\nu\nu)H$	1.6	2.6	1.3	1.3
All channels	0.95	1.89	2.1	2.1

between the signal strengths for the separate WH and ZH production processes is shown. The two production modes are consistent with the SM expectation, within uncertainties. This figure contains slightly different information than the one on the left panel as some final states contain signal events that originate from both WH and ZH production processes. The WH process contributes approximately 20% of the Higgs boson signal event yields in the $Z(\nu\nu)H$ channel, resulting from events in which the lepton is outside the detector acceptance, and the $Z(\ell\ell)H$ process contributes less than 5% to the $W(\ell\nu)H$ channel when one of the leptons is outside the detector acceptance. The dependency of the combined signal strength on the value assumed for the Higgs boson mass is shown in the left panel of Fig. 8.

In the right panel of Fig. 8 the best-fit values for the κ_V and κ_b parameters are shown. The parameter κ_V quantifies the ratio of the measured Higgs boson couplings to vector bosons relative to the SM value. The parameter κ_b quantifies the ratio of the measured Higgs boson partial width into $b\bar{b}$ relative to the SM value. They are defined as: $\kappa_V^2 = \sigma_{\text{VH}}/\sigma_{\text{VH}}^{\text{SM}}$ and $\kappa_b^2 = \Gamma_{b\bar{b}}/\Gamma_{b\bar{b}}^{\text{SM}}$, with the SM scaling of the total width [66]. The measured couplings are consistent with the expectations from the standard model, within uncertainties.

8.1 Results for the dijet mass cross-check analysis

The left panel of Fig. 9 shows a weighted dijet invariant mass distribution for the combination of all channels, in all boost regions, in the combined 7 and 8 TeV data, using the event selection for the $m(\text{jj})$ cross-check analysis described in Section 5. For each channel, the relative event weight in each boost region is obtained from

the ratio of the expected number of signal events to the sum of expected signal and background events in a window of $m(jj)$ values between 105 and 150 GeV. The expected signal used corresponds to the production of the SM Higgs boson with a mass of 125 GeV. The weight for the highest-boost region is set to 1.0 and all other weights are adjusted proportionally. Figure 9 also shows the same weighted dijet invariant mass distribution with all backgrounds, except diboson production, subtracted. The data are consistent with the presence of a diboson signal from ZZ and WZ channels, with $Z \rightarrow b\bar{b}$, with a rate consistent with the standard model prediction from the MADGRAPH generator, together with a small excess consistent with the production of the standard model Higgs boson with a mass of 125 GeV. For the $m(jj)$ analysis, a fit to the dijet invariant mass distribution results in a measured Higgs boson signal strength, relative to that predicted by the standard model, of $\mu = 0.8 \pm 0.7$, with a local significance of 1.1 standard deviations with respect to the background-only hypothesis. For a Higgs boson of mass 125 GeV, the expected and observed 95% CL upper limits on the production cross section, relative to the standard model prediction, are 1.4 and 2.0, respectively.

8.2 Diboson signal extraction

As a validation of the multivariate technique, BDT discriminants are trained using the diboson sample as signal, and all other processes, including VH production (at the predicted standard model rate for a 125 GeV Higgs mass), as background. This is done for the 8 TeV dataset only. The observed excess of events for the combined WZ and ZZ processes, with $Z \rightarrow b\bar{b}$, differs by over 7 standard deviations from the event yield expectation from the background-only hypothesis. The corresponding signal strength, relative to the prediction from the diboson MADGRAPH generator mentioned in Section 2, and rescaled to the cross section from the NLO MCFM generator, is measured to be $\mu_{VV} = 1.19^{+0.28}_{-0.23}$.

9 Summary

A search for the standard model Higgs boson when produced in association with an electroweak vector boson and decaying to $b\bar{b}$ is reported for the $W(\mu\nu)H$, $W(e\nu)H$, $W(\tau\nu)H$, $Z(\mu\mu)H$, $Z(ee)H$, and $Z(\nu\nu)H$ channels. The search is performed in data samples corresponding to integrated luminosities of up to 5.1 fb^{-1} at $\sqrt{s} = 7 \text{ TeV}$ and up to 18.9 fb^{-1} at $\sqrt{s} = 8 \text{ TeV}$, recorded by the CMS experiment at the LHC.

Upper limits, at the 95% confidence level, on the VH production cross section times the $H \rightarrow b\bar{b}$ branching fraction, with respect to the expectations for a standard model Higgs boson, are derived for the Higgs boson in the mass range 110–135 GeV. For a Higgs boson mass of 125 GeV the expected limit is 0.95 and the observed limit is 1.89.

An excess of events is observed above the expected background with a local significance of 2.1 standard deviations. The expected significance when taking into account the production of the standard model Higgs boson is also 2.1 standard deviations. The sensitivity of this search, as represented by the expected significance, is the highest for a single experiment thus far. The signal strength corresponding to this excess, relative to that of the standard model Higgs boson, is $\mu = 1.0 \pm 0.5$. The measurements presented in this article represent the first indication of the $H \rightarrow b\bar{b}$ decay at the LHC.

Acknowledgments

We congratulate our colleagues in the CERN accelerator departments for the excellent performance of the LHC and thank the technical and administrative staffs at CERN and at other CMS institutes for their contributions to the success of the CMS effort. In addition, we gratefully acknowledge the computing centres and personnel of the Worldwide LHC Computing Grid for delivering so effectively the computing infrastructure essential to our analyses. Finally, we acknowledge the enduring support for the construction and operation of the LHC and the CMS detector provided by the following funding agencies: the Austrian Federal Ministry of Science and Research and the Austrian Science Fund; the Belgian Fonds de la Recherche Scientifique, and Fonds voor Wetenschappelijk Onderzoek; the Brazilian Funding Agencies (CNPq, CAPES, FAPERJ, and FAPESP); the Bulgarian Ministry of Education and Science; CERN; the Chinese Academy of Sciences, Ministry of Science and Technology, and National Natural Science Foundation of China; the Colombian Funding Agency (COLCIENCIAS); the Croatian Ministry of Science, Education and Sport; the Research Promotion Foundation, Cyprus; the Ministry of Education and Research, Recurrent financing contract SF0690030s09 and European Regional Development Fund, Estonia; the Academy of Finland, Finnish Ministry of Education and Culture, and Helsinki Institute of Physics; the Institut National de Physique Nucléaire et de Physique des Particules / CNRS, and Commissariat à l'Énergie Atomique et aux Énergies Alternatives / CEA, France; the Bundesministerium

für Bildung und Forschung, Deutsche Forschungsgemeinschaft, and Helmholtz-Gemeinschaft Deutscher Forschungszentren, Germany; the General Secretariat for Research and Technology, Greece; the National Scientific Research Foundation, and National Office for Research and Technology, Hungary; the Department of Atomic Energy and the Department of Science and Technology, India; the Institute for Studies in Theoretical Physics and Mathematics, Iran; the Science Foundation, Ireland; the Istituto Nazionale di Fisica Nucleare, Italy; the Korean Ministry of Education, Science and Technology and the World Class University program of NRF, Republic of Korea; the Lithuanian Academy of Sciences; the Mexican Funding Agencies (CINVESTAV, CONACYT, SEP, and UASLP-FAI); the Ministry of Business, Innovation and Employment, New Zealand; the Pakistan Atomic Energy Commission; the Ministry of Science and Higher Education and the National Science Centre, Poland; the Fundação para a Ciência e a Tecnologia, Portugal; JINR, Dubna; the Ministry of Education and Science of the Russian Federation, the Federal Agency of Atomic Energy of the Russian Federation, Russian Academy of Sciences, and the Russian Foundation for Basic Research; the Ministry of Education, Science and Technological Development of Serbia; the Secretaría de Estado de Investigación, Desarrollo e Innovación and Programa Consolider-Ingenio 2010, Spain; the Swiss Funding Agencies (ETH Board, ETH Zurich, PSI, SNF, UniZH, Canton Zurich, and SER); the National Science Council, Taipei; the Thailand Center of Excellence in Physics, the Institute for the Promotion of Teaching Science and Technology of Thailand, Special Task Force for Activating Research and the National Science and Technology Development Agency of Thailand; the Scientific and Technical Research Council of Turkey, and Turkish Atomic Energy Authority; the Science and Technology Facilities Council, UK; the US Department of Energy, and the US National Science Foundation.

Individuals have received support from the Marie-Curie programme and the European Research Council and EPLANET (European Union); the Leventis Foundation; the A. P. Sloan Foundation; the Alexander von Humboldt Foundation; the Belgian Federal Science Policy Office; the Fonds pour la Formation à la Recherche dans l'Industrie et dans l'Agriculture (FRIA-Belgium); the Agentschap voor Innovatie door Wetenschap en Technologie (IWT-Belgium); the Ministry of Education, Youth and Sports (MEYS) of Czech Republic; the Council of Science and Industrial Research, India; the Compagnia di San Paolo (Torino); the HOMING PLUS programme of Foundation for Polish Science, cofinanced by EU, Regional Development Fund; and the Thalís and Aristeia programmes cofinanced by EU-ESF and the Greek NSRF.

References

- [1] CMS Collaboration, “Observation of a new boson at a mass of 125 GeV with the CMS experiment at the LHC”, *Phys. Lett. B* **716** (2012) 30, [doi:10.1016/j.physletb.2012.08.021](https://doi.org/10.1016/j.physletb.2012.08.021), [arXiv:1207.7235](https://arxiv.org/abs/1207.7235).
- [2] ATLAS Collaboration, “Observation of a new particle in the search for the Standard Model Higgs boson with the ATLAS detector at the LHC”, *Phys. Lett. B* **716** (2012) 1, [doi:10.1016/j.physletb.2012.08.020](https://doi.org/10.1016/j.physletb.2012.08.020), [arXiv:1207.7214](https://arxiv.org/abs/1207.7214).
- [3] F. Englert and R. Brout, “Broken symmetry and the mass of gauge vector mesons”, *Phys. Rev. Lett.* **13** (1964) 321, [doi:10.1103/PhysRevLett.13.321](https://doi.org/10.1103/PhysRevLett.13.321).
- [4] P. W. Higgs, “Broken symmetries, massless particles and gauge fields”, *Phys. Lett.* **12** (1964) 132, [doi:10.1016/0031-9163\(64\)91136-9](https://doi.org/10.1016/0031-9163(64)91136-9).
- [5] P. W. Higgs, “Broken symmetries and the masses of gauge bosons”, *Phys. Rev. Lett.* **13** (1964) 508, [doi:10.1103/PhysRevLett.13.508](https://doi.org/10.1103/PhysRevLett.13.508).
- [6] G. S. Guralnik, C. R. Hagen, and T. W. B. Kibble, “Global conservation laws and massless particles”, *Phys. Rev. Lett.* **13** (1964) 585, [doi:10.1103/PhysRevLett.13.585](https://doi.org/10.1103/PhysRevLett.13.585).
- [7] P. W. Higgs, “Spontaneous symmetry breakdown without massless bosons”, *Phys. Rev.* **145** (1966) 1156, [doi:10.1103/PhysRev.145.1156](https://doi.org/10.1103/PhysRev.145.1156).
- [8] T. W. B. Kibble, “Symmetry breaking in non-Abelian gauge theories”, *Phys. Rev.* **155** (1967) 1554, [doi:10.1103/PhysRev.155.1554](https://doi.org/10.1103/PhysRev.155.1554).
- [9] LHC Higgs Cross Section Working Group Collaboration, “Handbook of LHC Higgs Cross Sections: 1. Inclusive Observables”, (2011). [arXiv:1101.0593](https://arxiv.org/abs/1101.0593).
- [10] CDF and D0 Collaborations, “Higgs boson studies at the Tevatron”, *Phys. Rev. D* **88** (2013) 052014, [doi:10.1103/PhysRevD.88.052014](https://doi.org/10.1103/PhysRevD.88.052014).
- [11] CDF and D0 Collaborations, “Evidence for a particle produced in association with weak bosons and decaying to a bottom-antibottom quark pair in Higgs boson searches at the Tevatron”, *Phys. Rev. Lett.* **109** (2012) 071804, [doi:10.1103/PhysRevLett.109.071804](https://doi.org/10.1103/PhysRevLett.109.071804), [arXiv:1207.6436](https://arxiv.org/abs/1207.6436).

- [12] ATLAS Collaboration, “Search for the Standard Model Higgs boson produced in association with a vector boson and decaying to a b -quark pair with the ATLAS detector”, *Phys. Lett. B* **718** (2012) 369, [doi:10.1016/j.physletb.2012.10.061](https://doi.org/10.1016/j.physletb.2012.10.061), [arXiv:1207.0210](https://arxiv.org/abs/1207.0210).
- [13] CMS Collaboration, “Observation of a new boson with mass near 125 GeV in pp collisions at $\sqrt{s} = 7$ TeV and 8 TeV”, *JHEP* **06** (2013) 081, [doi:10.1007/JHEP06\(2013\)081](https://doi.org/10.1007/JHEP06(2013)081), [arXiv:1303.4571](https://arxiv.org/abs/1303.4571).
- [14] B. P. Roe et al., “Boosted decision trees, an alternative to artificial neural networks”, *Nucl. Instrum. Meth. A* **543** (2005) 577, [doi:10.1016/j.nima.2004.12.018](https://doi.org/10.1016/j.nima.2004.12.018), [arXiv:physics/0408124](https://arxiv.org/abs/physics/0408124).
- [15] A. Hocker et al., “TMVA—Toolkit for Multivariate Data Analysis”, *PoS ACAT* (2007) 040, [arXiv:physics/0703039](https://arxiv.org/abs/physics/0703039).
- [16] CMS Collaboration, “The CMS experiment at the CERN LHC”, *JINST* **3** (2008) S08004, [doi:10.1088/1748-0221/3/08/S08004](https://doi.org/10.1088/1748-0221/3/08/S08004).
- [17] GEANT4 Collaboration, “GEANT4—a simulation toolkit”, *Nucl. Instrum. Meth. A* **506** (2003) 250, [doi:10.1016/S0168-9002\(03\)01368-8](https://doi.org/10.1016/S0168-9002(03)01368-8).
- [18] S. Frixione, P. Nason, and C. Oleari, “Matching NLO QCD computations with parton shower simulations: the POWHEG method”, *JHEP* **11** (2007) 070, [doi:10.1088/1126-6708/2007/11/070](https://doi.org/10.1088/1126-6708/2007/11/070), [arXiv:0709.2092](https://arxiv.org/abs/0709.2092).
- [19] J. Alwall et al., “MadGraph 5: going beyond”, *JHEP* **06** (2011) 128, [doi:10.1007/JHEP06\(2011\)128](https://doi.org/10.1007/JHEP06(2011)128), [arXiv:1106.0522](https://arxiv.org/abs/1106.0522).
- [20] T. Sjöstrand, S. Mrenna, and P. Z. Skands, “PYTHIA 6.4 physics and manual”, *JHEP* **05** (2006) 026, [doi:10.1088/1126-6708/2006/05/026](https://doi.org/10.1088/1126-6708/2006/05/026), [arXiv:hep-ph/0603175](https://arxiv.org/abs/hep-ph/0603175).
- [21] J. M. Campbell and R. K. Ellis, “MCFM for the Tevatron and the LHC”, *Nucl. Phys. Proc. Suppl.* **205-206** (2010) 10, [doi:10.1016/j.nuclphysbps.2010.08.011](https://doi.org/10.1016/j.nuclphysbps.2010.08.011), [arXiv:1007.3492](https://arxiv.org/abs/1007.3492).
- [22] R. Gavin, Y. Li, F. Petriello, and S. Quackenbush, “FEWZ 2.0: A code for hadronic Z production at next-to-next-to-leading order”, *Comput. Phys. Commun.* **182** (2011) 2388, [doi:10.1016/j.cpc.2011.06.008](https://doi.org/10.1016/j.cpc.2011.06.008), [arXiv:1011.3540](https://arxiv.org/abs/1011.3540).

- [23] Y. Li and F. Petriello, “Combining QCD and electroweak corrections to dilepton production in FEWZ”, *Phys. Rev. D* **86** (2012) 094034, [doi:10.1103/PhysRevD.86.094034](https://doi.org/10.1103/PhysRevD.86.094034), [arXiv:1208.5967](https://arxiv.org/abs/1208.5967).
- [24] R. Gavin, Y. Li, F. Petriello, and S. Quackenbush, “W Physics at the LHC with FEWZ 2.1”, *Comput. Phys. Commun.* **184** (2013) 208, [doi:10.1016/j.cpc.2012.09.005](https://doi.org/10.1016/j.cpc.2012.09.005), [arXiv:1201.5896](https://arxiv.org/abs/1201.5896).
- [25] A. D. Martin, W. J. Stirling, R. S. Thorne, and G. Watt, “Parton distributions for the LHC”, *Eur. Phys. J. C* **63** (2009) 189, [doi:10.1140/epjc/s10052-009-1072-5](https://doi.org/10.1140/epjc/s10052-009-1072-5), [arXiv:0901.0002](https://arxiv.org/abs/0901.0002).
- [26] J. Pumplin et al., “New generation of parton distributions with uncertainties from global QCD analysis”, *JHEP* **07** (2002) 012, [doi:10.1088/1126-6708/2002/07/012](https://doi.org/10.1088/1126-6708/2002/07/012), [arXiv:hep-ph/0201195](https://arxiv.org/abs/hep-ph/0201195).
- [27] M. Bähr et al., “Herwig++ physics and manual”, *Eur. Phys. J. C* **58** (2008) 639, [doi:10.1140/epjc/s10052-008-0798-9](https://doi.org/10.1140/epjc/s10052-008-0798-9), [arXiv:0803.0883](https://arxiv.org/abs/0803.0883).
- [28] CMS Collaboration, “Measurement of the underlying event activity at the LHC with $\sqrt{s} = 7$ TeV and comparison with $\sqrt{s} = 0.9$ TeV”, *JHEP* **09** (2011) 109, [doi:10.1007/JHEP09\(2011\)109](https://doi.org/10.1007/JHEP09(2011)109), [arXiv:1107.0330](https://arxiv.org/abs/1107.0330).
- [29] S. Jadach, J. H. Kühn, and Z. Was, “TAUOLA—a library of Monte Carlo programs to simulate decays of polarized tau leptons”, *Comput. Phys. Commun.* **64** (1991) 275, [doi:10.1016/0010-4655\(91\)90038-M](https://doi.org/10.1016/0010-4655(91)90038-M).
- [30] CMS Collaboration, “Particle-Flow Event Reconstruction in CMS and Performance for Jets, Taus, and E_T^{miss} ”, CMS Physics Analysis Summary CMS-PAS-PFT-09-001, (2009).
- [31] CMS Collaboration, “Commissioning of the Particle-flow Event Reconstruction in Minimum-Bias and Jet Events from pp Collisions at 7 TeV”, CMS Physics Analysis Summary CMS-PAS-PFT-10-002, (2010).
- [32] M. Cacciari and G. P. Salam, “Pileup subtraction using jet areas”, *Phys. Lett. B* **659** (2008) 119, [doi:10.1016/j.physletb.2007.09.077](https://doi.org/10.1016/j.physletb.2007.09.077), [arXiv:0707.1378](https://arxiv.org/abs/0707.1378).
- [33] M. Cacciari, G. P. Salam and G. Soyez, “The anti- k_t jet clustering algorithm”, *JHEP* **04** (2008) 063, [doi:10.1088/1126-6708/2008/04/063](https://doi.org/10.1088/1126-6708/2008/04/063), [arXiv:0802.1189](https://arxiv.org/abs/0802.1189).

- [34] M. Cacciari, G. P. Salam, and G. Soyez, “FastJet User Manual”, *Eur. Phys. J. C* **72** (2012) 1896, doi:[10.1140/epjc/s10052-012-1896-2](https://doi.org/10.1140/epjc/s10052-012-1896-2), [arXiv:1111.6097](https://arxiv.org/abs/1111.6097).
- [35] M. Cacciari and G. P. Salam, “Dispelling the N^3 myth for the k_t jet-finder”, *Phys. Lett. B* **641** (2006) 57, doi:[10.1016/j.physletb.2006.08.037](https://doi.org/10.1016/j.physletb.2006.08.037), [arXiv:hep-ph/0512210](https://arxiv.org/abs/hep-ph/0512210).
- [36] CMS Collaboration, “Determination of jet energy calibration and transverse momentum resolution in CMS”, *JINST* **6** (2011) P11002, doi:[10.1088/1748-0221/6/11/P11002](https://doi.org/10.1088/1748-0221/6/11/P11002), [arXiv:1107.4277](https://arxiv.org/abs/1107.4277).
- [37] CMS Collaboration, “Performance of CMS muon reconstruction in pp collision events at $\sqrt{7}$ TeV”, *JINST* **7** (2012) P10002, doi:[10.1088/1748-0221/7/10/P10002](https://doi.org/10.1088/1748-0221/7/10/P10002), [arXiv:1206.4071](https://arxiv.org/abs/1206.4071).
- [38] CMS Collaboration, “Electron reconstruction and identification at $\sqrt{s} = 7$ TeV”, CMS Physics Analysis Summary CMS-PAS-EGM-10-004, (2010).
- [39] CMS Collaboration, “Performance of tau-lepton reconstruction and identification in CMS”, *JINST* **7** (2012) P01001, doi:[10.1088/1748-0221/7/01/P01001](https://doi.org/10.1088/1748-0221/7/01/P01001), [arXiv:1109.6034](https://arxiv.org/abs/1109.6034).
- [40] CMS Collaboration, “Identification of b-quark jets with the CMS experiment”, *JINST* **8** (2013) P04013, doi:[10.1088/1748-0221/8/04/P04013](https://doi.org/10.1088/1748-0221/8/04/P04013), [arXiv:1211.4462](https://arxiv.org/abs/1211.4462).
- [41] J. M. Butterworth, A. R. Davison, M. Rubin, and G. P. Salam, “Jet Substructure as a New Higgs-Search Channel at the Large Hadron Collider”, *Phys. Rev. Lett.* **100** (2008) 242001, doi:[10.1103/PhysRevLett.100.242001](https://doi.org/10.1103/PhysRevLett.100.242001).
- [42] T. Aaltonen et al., “Improved b -jet Energy Correction for $H \rightarrow b\bar{b}$ Searches at CDF”, (2011). [arXiv:1107.3026](https://arxiv.org/abs/1107.3026).
- [43] W. Verkerke and D. P. Kirkby, “The RooFit toolkit for data modeling”, in *Computing in High Energy and Nuclear Physics, CHEP03*. 2003. [arXiv:physics/0306116](https://arxiv.org/abs/physics/0306116). eConf/C0303241/MOLT007.
- [44] CDF Collaboration, “Search for the standard model Higgs boson decaying to a $b\bar{b}$ pair in events with two oppositely-charged leptons using the full

- CDF data set", *Phys. Rev. Lett.* **109** (2012) 111803,
[doi:10.1103/PhysRevLett.109.111803](#), [arXiv:1207.1704](#).
- [45] J. Gallicchio and M. D. Schwartz, "Seeing in Color: Jet Superstructure",
Phys. Rev. Lett. **105** (2010) 022001,
[doi:10.1103/PhysRevLett.105.022001](#), [arXiv:1001.5027](#).
- [46] ATLAS Collaboration, "Measurement of the cross-section for W boson production in association with b-jets in pp collisions at $\sqrt{s} = 7$ TeV with the ATLAS detector", *JHEP* **06** (2013) 084,
[doi:10.1007/JHEP06\(2013\)084](#), [arXiv:1302.2929](#).
- [47] CMS Collaboration, "Measurement of the cross section and angular correlations for associated production of a Z boson with b hadrons in pp collisions at $\sqrt{s} = 7$ TeV", (2013). [arXiv:1310.1349](#). Submitted to JHEP.
- [48] CMS Collaboration, "Measurement of the $Z/\gamma^{**}+b$ -jet cross section in pp collisions at 7 TeV", *JHEP* **06** (2012) 126,
[doi:10.1007/JHEP06\(2012\)126](#), [arXiv:1204.1643](#).
- [49] CMS Collaboration, "Absolute Calibration of the Luminosity Measurement at CMS: Winter 2012 Update", CMS Physics Analysis Summary CMS-PAS-SMP-12-008, (2012).
- [50] CMS Collaboration, "CMS Luminosity Measurement Based on Pixel Cluster Counting: Summer 2012 Update", CMS Physics Analysis Summary CMS-PAS-LUM-12-001, (2012).
- [51] S. Dittmaier et al., "Handbook of LHC Higgs Cross Sections: 2. Differential Distributions", CERN Report CERN-2012-002, (2012).
- [52] S. Alekhin et al., "The PDF4LHC Working Group Interim Report", (2011).
[arXiv:1101.0536](#).
- [53] M. Botje et al., "The PDF4LHC Working Group Interim Recommendations", (2011). [arXiv:1101.0538](#).
- [54] H.-L. Lai et al., "New parton distributions for collider physics", *Phys. Rev. D* **82** (2010) 074024, [doi:10.1103/PhysRevD.82.074024](#),
[arXiv:1007.2241](#).

- [55] R. D. Ball et al., “Impact of Heavy Quark Masses on Parton Distributions and LHC Phenomenology”, *Nucl. Phys. B* **849** (2011) 296, [doi:10.1016/j.nuclphysb.2011.03.021](https://doi.org/10.1016/j.nuclphysb.2011.03.021), [arXiv:1101.1300](https://arxiv.org/abs/1101.1300).
- [56] M. Ciccolini, A. Denner, and S. Dittmaier, “Strong and electroweak corrections to the production of Higgs+2jets via weak interactions at the LHC”, *Phys. Rev. Lett.* **99** (2007) 161803, [doi:10.1103/PhysRevLett.99.161803](https://doi.org/10.1103/PhysRevLett.99.161803), [arXiv:0707.0381](https://arxiv.org/abs/0707.0381).
- [57] M. Ciccolini, A. Denner, and S. Dittmaier, “Electroweak and QCD corrections to Higgs production via vector-boson fusion at the LHC”, *Phys. Rev. D* **77** (2008) 013002, [doi:10.1103/PhysRevD.77.013002](https://doi.org/10.1103/PhysRevD.77.013002), [arXiv:0710.4749](https://arxiv.org/abs/0710.4749).
- [58] A. Denner, S. Dittmaier, S. Kallweit, and A. Muck, “Electroweak corrections to Higgs-strahlung off W/Z bosons at the Tevatron and the LHC with HAWK”, *JHEP* **03** (2012) 075, [doi:10.1007/JHEP03\(2012\)075](https://doi.org/10.1007/JHEP03(2012)075), [arXiv:1112.5142](https://arxiv.org/abs/1112.5142).
- [59] G. Ferrera, M. Grazzini, and F. Tramontano, “Associated WH production at hadron colliders: a fully exclusive QCD calculation at NNLO”, *Phys. Rev. Lett.* **107** (2011) 152003, [doi:10.1103/PhysRevLett.107.152003](https://doi.org/10.1103/PhysRevLett.107.152003), [arXiv:1107.1164](https://arxiv.org/abs/1107.1164).
- [60] S. Frixione and B. R. Webber, “Matching NLO QCD computations and parton shower simulations”, *JHEP* **06** (2002) 029, [doi:10.1088/1126-6708/2002/06/029](https://doi.org/10.1088/1126-6708/2002/06/029), [arXiv:hep-ph/0204244](https://arxiv.org/abs/hep-ph/0204244).
- [61] CMS Collaboration, “Measurement of the single-top-quark t -channel cross section in pp collisions at $\sqrt{s} = 7$ TeV”, *JHEP* **12** (2012) 035, [doi:10.1007/JHEP12\(2012\)035](https://doi.org/10.1007/JHEP12(2012)035), [arXiv:1209.4533](https://arxiv.org/abs/1209.4533).
- [62] CMS Collaboration, “Measurement of the W^+W^- and ZZ production cross sections in pp collisions at $\sqrt{s} = 8$ TeV”, *Phys. Lett. B* **721** (2013) 190, [doi:10.1016/j.physletb.2013.03.027](https://doi.org/10.1016/j.physletb.2013.03.027).
- [63] A. L. Read, “Presentation of search results: The CL_s technique”, *J. Phys. G* **28** (2002) 2693, [doi:10.1088/0954-3899/28/10/313](https://doi.org/10.1088/0954-3899/28/10/313).
- [64] T. Junk, “Confidence level computation for combining searches with small statistics”, *Nucl. Instrum. Meth. A* **434** (1999) 435, [doi:10.1016/S0168-9002\(99\)00498-2](https://doi.org/10.1016/S0168-9002(99)00498-2).

- [65] [ATLAS and CMS Collaborations, LHC Higgs Combination Group, “Procedure for the LHC Higgs boson search combination in Summer 2011”, ATL-PHYS-PUB 011-11/CMS NOTE 2011-005, \(2011\).](#)
- [66] S. Heinmeyer et al., “Handbook of LHC Higgs Cross Sections: 3. Higgs Properties”, CERN Report CERN-2013-004, (2013).

A Post-fit BDT distributions

Figures 10–14 show all the post-fit BDT distributions, for the $m_H = 125$ GeV training, for all channels and for all boost regions. In order to better display the different shapes of the signal and background BDT distributions, Fig. 15 shows these distributions for the highest-boost region in each channel, normalized to unity. See Section 8 for more details.

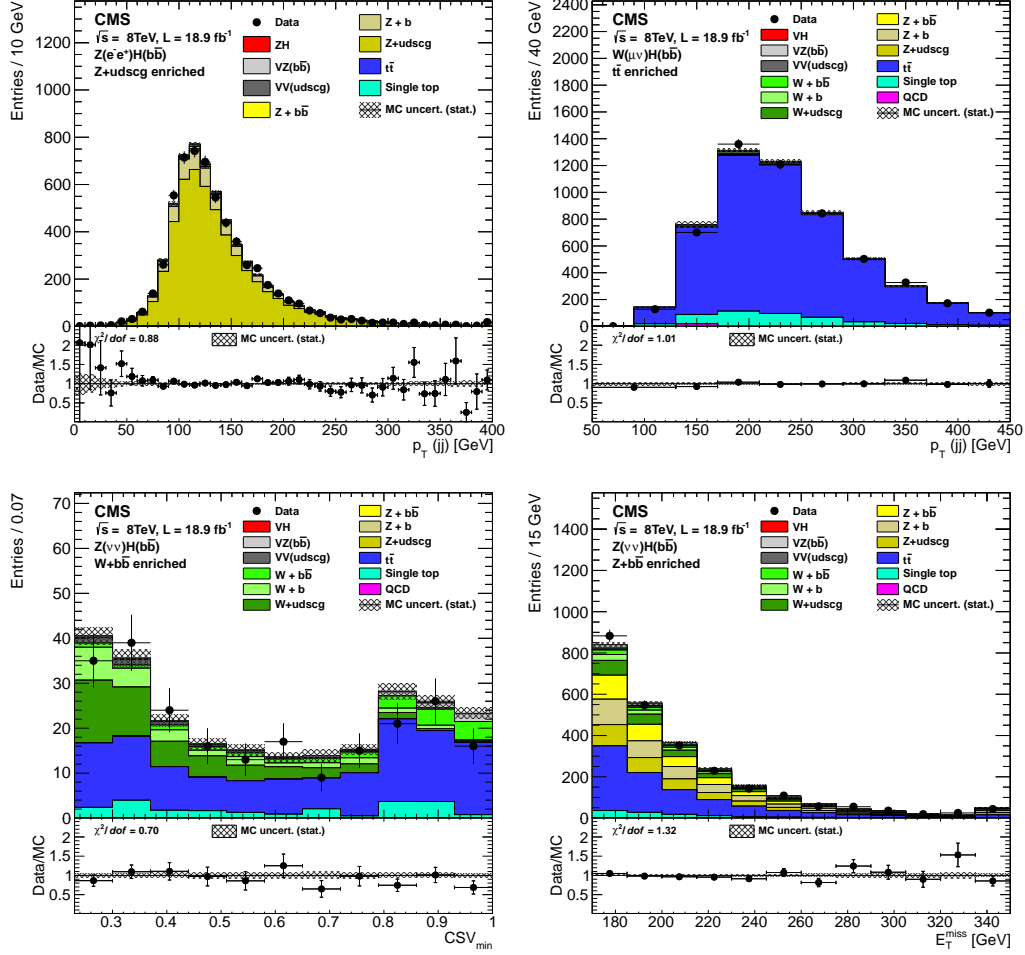


Figure 2: Examples of distributions for variables in the simulated samples and in data for different control regions and for different channels after applying the data/MC scale factors in Table 7. Top left: Dijet p_T distribution in the Z+jets control region for the Z(ee)H channel. Top right: p_T distribution in the $t\bar{t}$ control region for the W($\mu\nu$)H channel. Bottom left: CSV_{min} distribution for the W+HF high-boost control region for the Z($\nu\nu$)H channel. Bottom right: E_T^{miss} distribution for the Z+HF high-boost control region for the Z($\nu\nu$)H channel. The bottom inset in each figure shows the ratio of the number of events observed in data to that of the Monte Carlo prediction for signal and backgrounds.

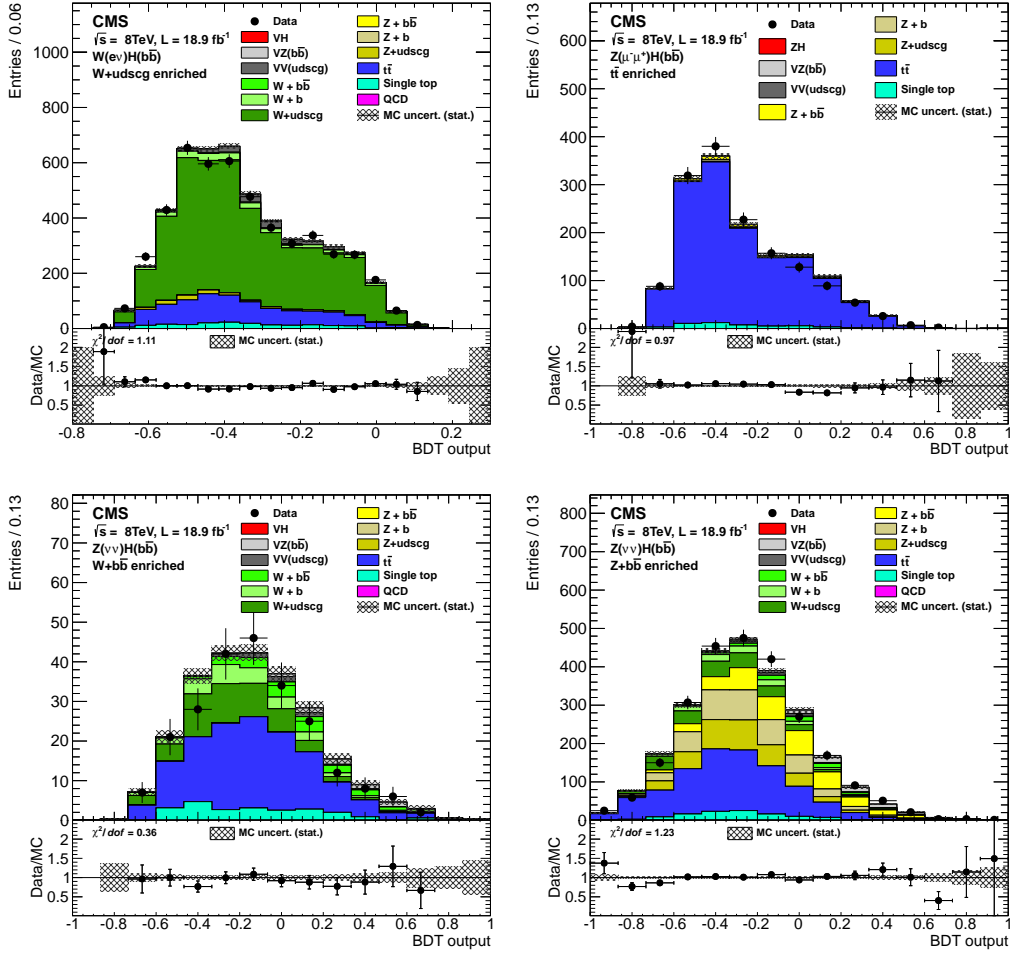


Figure 3: Examples of distributions of the event BDT discriminant output in the simulated samples and in data for different control regions and for different channels after applying the data/MC scale factors in Table 7. Top left: W+jets control region for the $W(e\nu)H$ channel. Top right: $t\bar{t}$ control region for the $Z(\mu\mu)H$ channel. Bottom left: W+HF high-boost control region for the $Z(\nu\nu)H$ channel. Bottom right: Z+HF high-boost control region for the $Z(\nu\nu)H$ channel. The bottom inset in each figure shows the ratio of the number of events observed in data to that of the Monte Carlo prediction for signal and backgrounds.

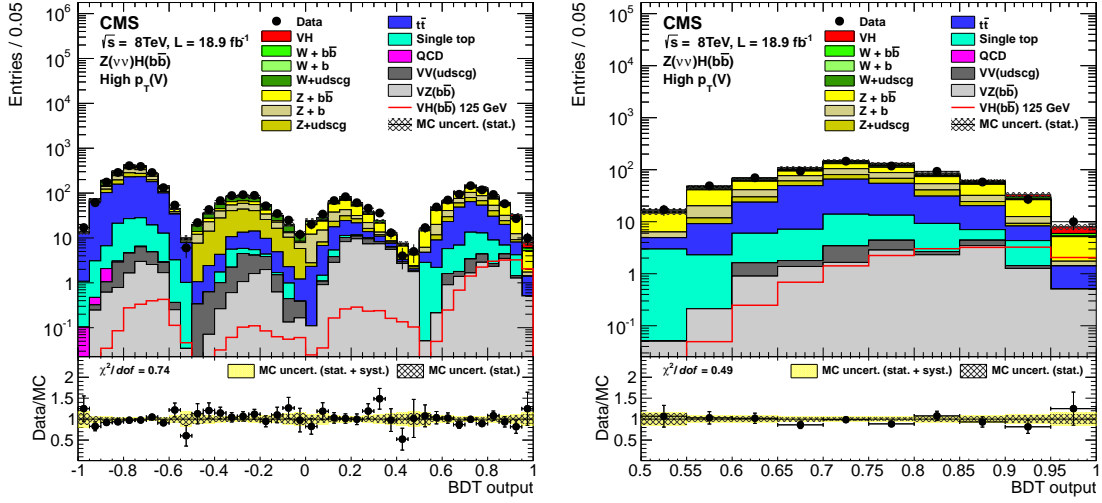


Figure 4: Post-fit BDT output distributions for $Z(\nu\nu)H$ in the high-boost region for 8 TeV data (points with error bars), all backgrounds, and signal, after all selection criteria have been applied. The event BDT discriminant values for events in the four different subsets are rescaled and offset to assemble a single BDT output variable. This leads to the four equally-sized partitions shown in the left panel. The partitions correspond, starting from the left, to the event subsets enriched in $t\bar{t}$, V +jets, diboson, and VH production. The right panel shows the right-most, VH -enriched, partition in more detail. The bottom inset in each figure shows the ratio of the number of events observed in data to that of the Monte Carlo prediction for signal and backgrounds.

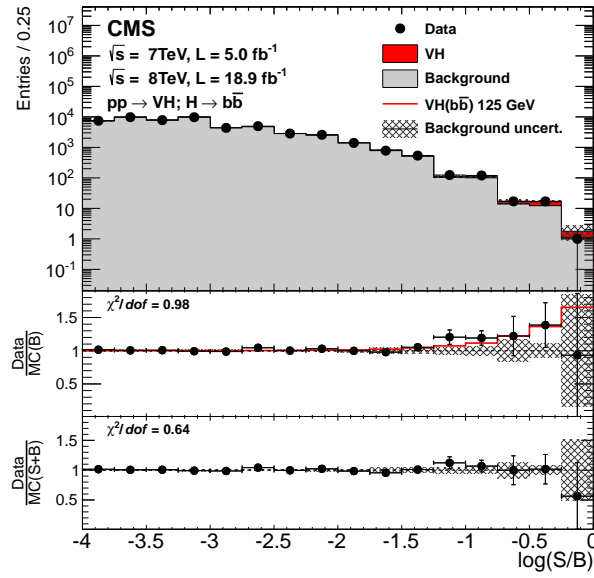


Figure 5: Combination of all channels into a single distribution. Events are sorted in bins of similar expected signal-to-background ratio, as given by the value of the output of their corresponding BDT discriminant (trained with a Higgs boson mass hypothesis of 125 GeV). The two bottom insets show the ratio of the data to the background-only prediction (above) and to the predicted sum of background and SM Higgs boson signal with a mass of 125 GeV (below).

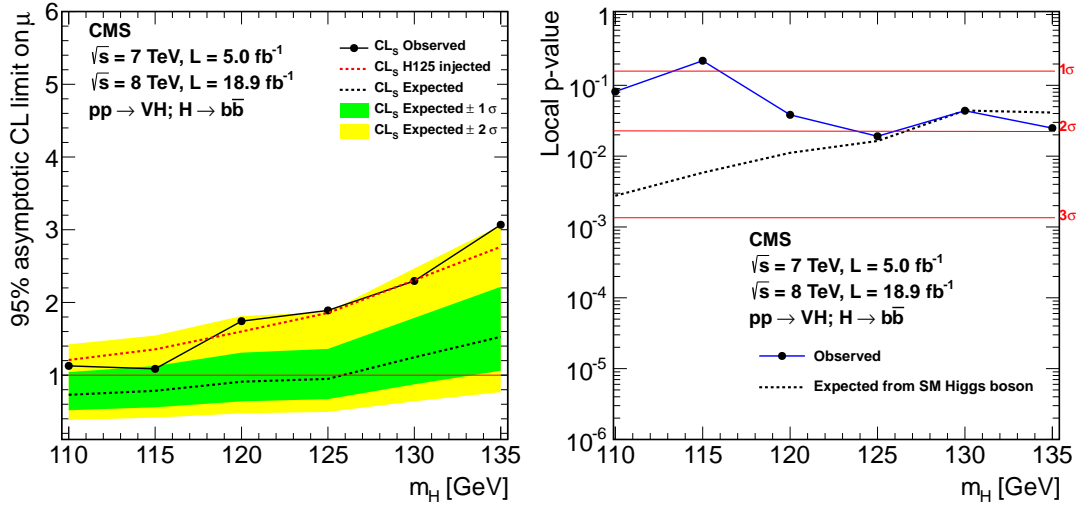


Figure 6: Left: The expected and observed 95% CL upper limits on the product of the VH production cross section times the $H \rightarrow b\bar{b}$ branching fraction, with respect to the expectations for the standard model Higgs boson. The limits are obtained combining the results of the searches using the 2011 (7 TeV) and 2012 (8 TeV) data. The red dashed line represents the expected limit obtained from the sum of expected backgrounds and the SM Higgs boson signal with a mass of 125 GeV. Right: local p-values and corresponding significance (measured in standard deviations) for the background-only hypothesis to account for the observed excess of events in the data.

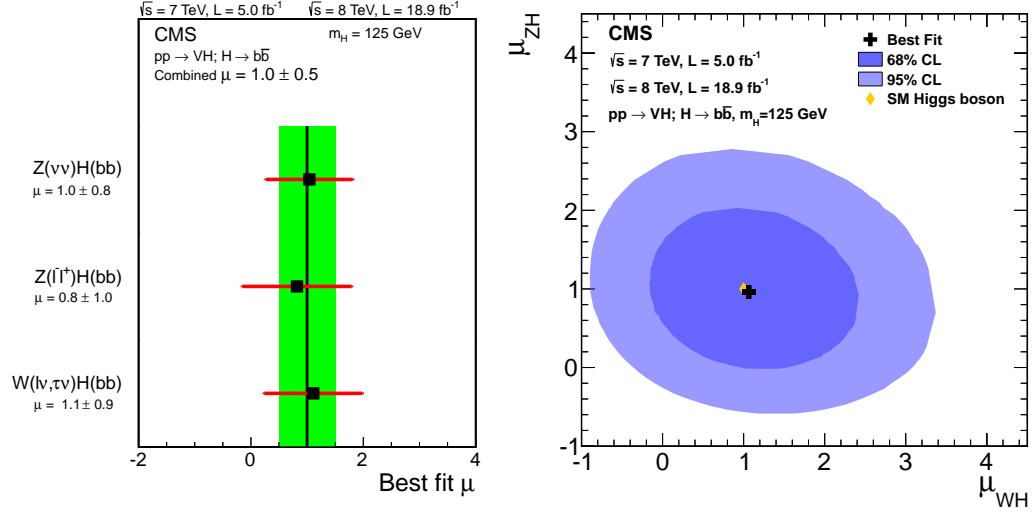


Figure 7: Left: The best-fit value of the production cross section for a 125 GeV Higgs boson relative to the standard model cross section, i.e., signal strength μ , for partial combinations of channels and for all channels combined (band). Right: The best-fit values and the 68% and 95% CL contour regions for the μ_{ZH} , μ_{WH} signal strength parameters for a 125 GeV Higgs boson.

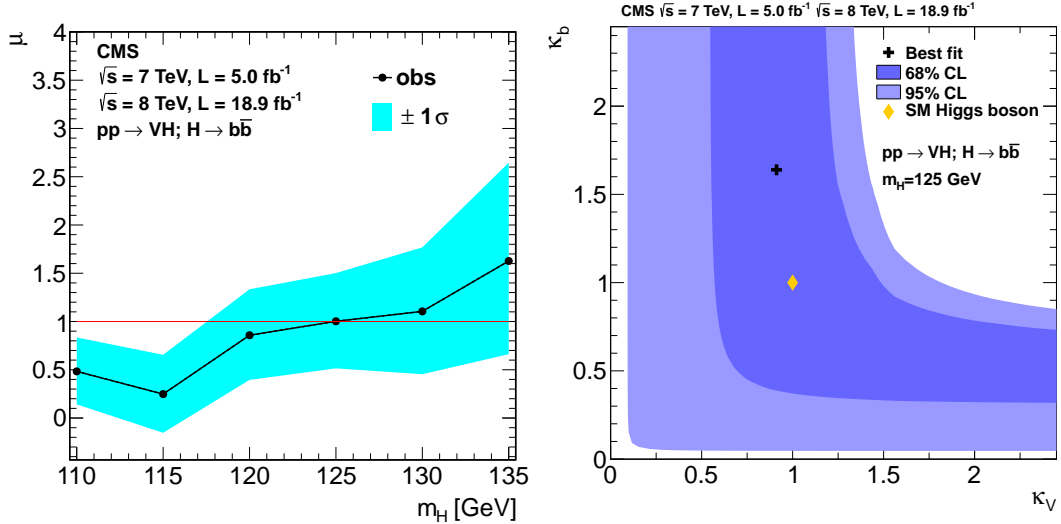


Figure 8: Left: Signal strength for all channels combined as a function of the value assumed for the Higgs boson mass. Right: The best-fit values and the 68% and 95% CL contour regions for the κ_V and κ_b parameters. The cross indicates the best-fit values and the yellow diamond shows the SM point $(\kappa_V, \kappa_b) = (1, 1)$. The likelihood fit is performed in the positive quadrant only.

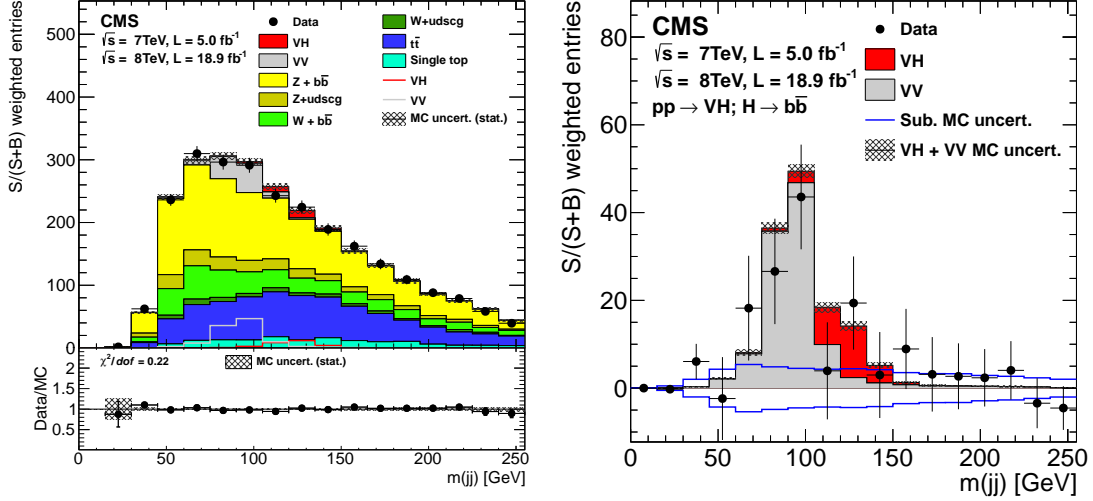


Figure 9: Dijet mass cross-check analysis. Left: weighted dijet invariant mass distribution, combined for all channels. For each channel, the relative dijet mass distribution weight for each boost region is obtained from the ratio of the expected number of signal events to the sum of expected signal and background events in a window of $m(jj)$ values between 105 and 150 GeV. The expected signal used corresponds to the production of the SM Higgs boson with a mass of 125 GeV. The weight for the highest-boost region is set to 1.0 and all other weights are adjusted proportionally. The solid histograms for the backgrounds and the signal are summed cumulatively. The line histogram for signal and for VV backgrounds are also shown superimposed. The data is represented by points. The bottom inset shows the ratio of the number of events observed in data to that of the Monte Carlo prediction for signal and backgrounds. Right: same distribution with all backgrounds, except dibosons, subtracted.

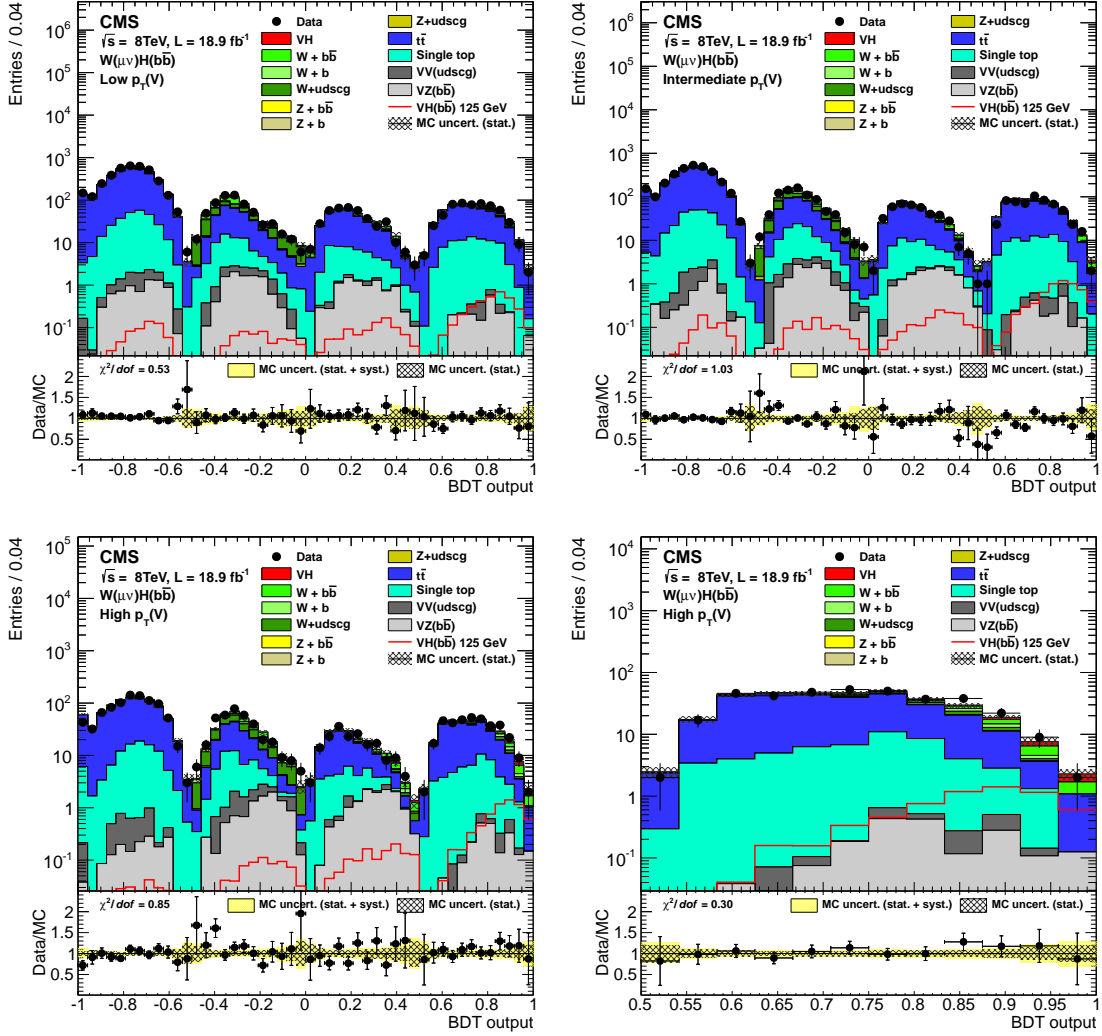


Figure 10: Post-fit BDT output distributions for $W(\mu\nu)H$ in the low-boost region (left), the intermediate-boost (right), and the high-boost (bottom), for 8 TeV data (points with error bars), all backgrounds, and signal, after all selection criteria have been applied. Bottom right: the VH-enriched partition of the high-boost region is shown in more detail. The bottom inset in each figure shows the ratio of the number of events observed in data to that of the Monte Carlo prediction for signal and backgrounds.

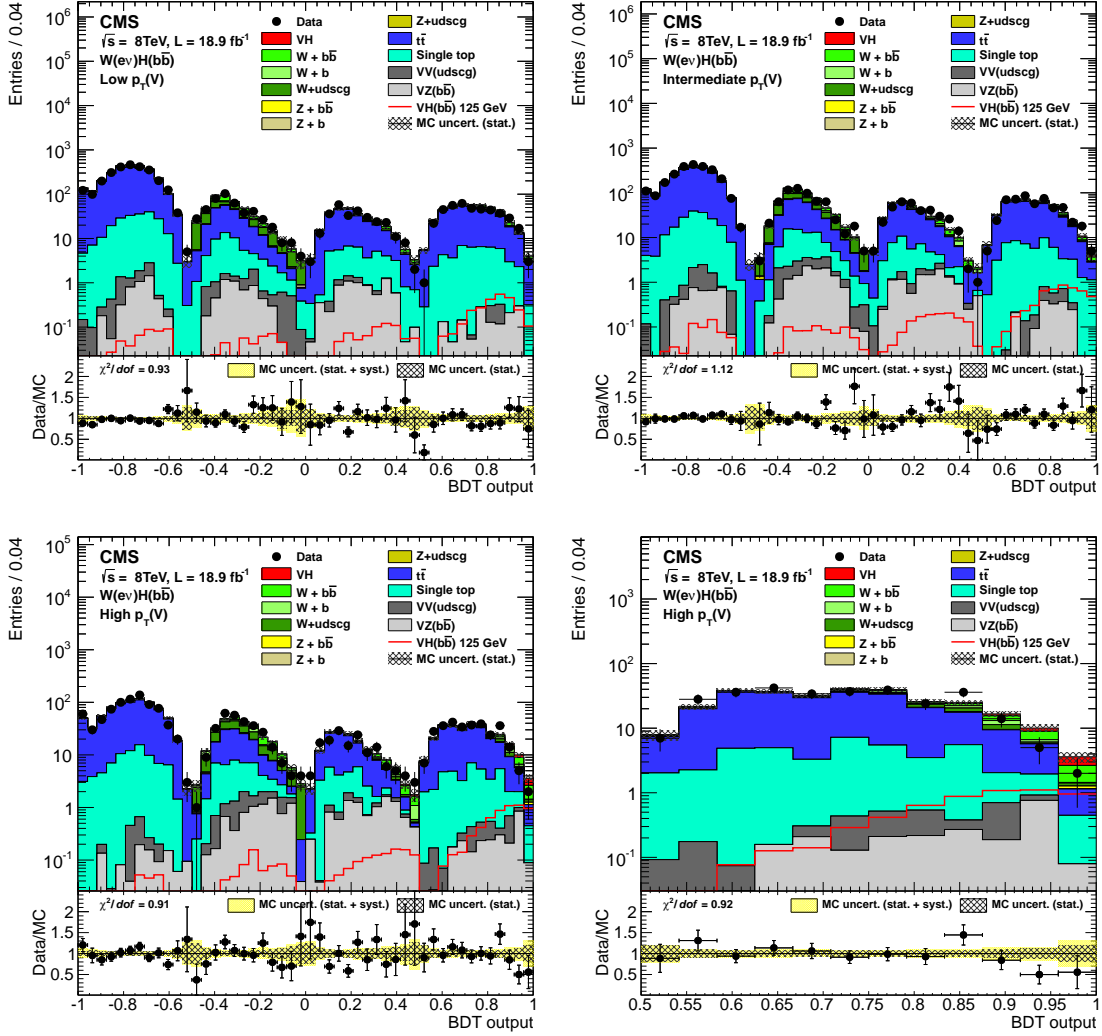


Figure 11: Post-fit BDT output distributions for $W(e\nu)H$ in the low-boost region (left), the intermediate-boost (right), and the high-boost (bottom), for 8 TeV data (points with error bars), all backgrounds, and signal, after all selection criteria have been applied. Bottom right: the VH-enriched partition of the high-boost region is shown in more detail. The bottom inset in each figure shows the ratio of the number of events observed in data to that of the Monte Carlo prediction for signal and backgrounds.

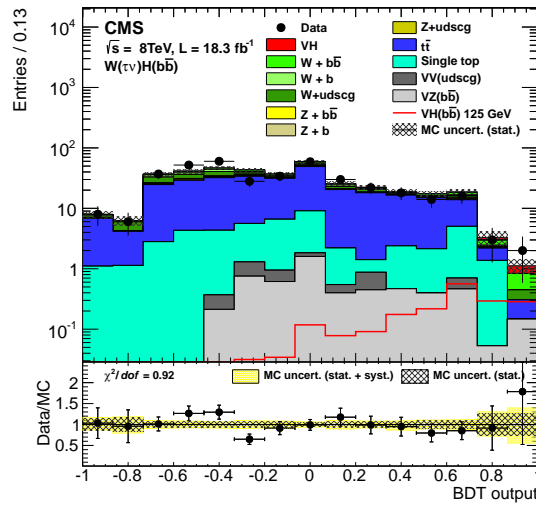


Figure 12: Post-fit BDT output distributions for $W(\tau\nu)H$ for 8 TeV data (points with error bars), all backgrounds, and signal, after all selection criteria have been applied. The bottom inset shows the ratio of the number of events observed in data to that of the Monte Carlo prediction for signal and backgrounds.

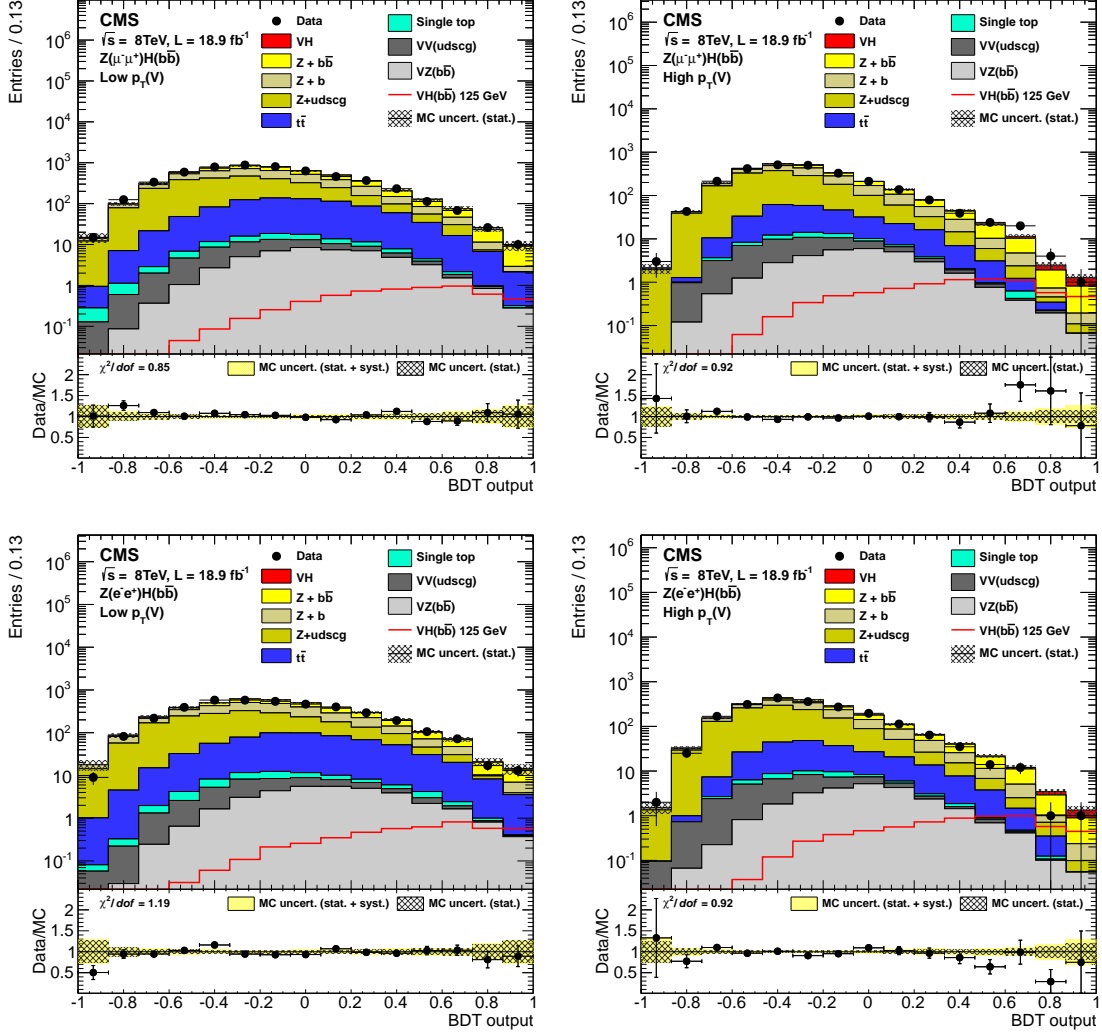


Figure 13: Post-fit BDT output distributions for $Z(\ell\ell)H$ in the low-boost region (left) and high-boost region (right), for 8 TeV data (points with error bars), all backgrounds, and signal, after all selection criteria have been applied. Top: $Z(\mu\mu)H$, bottom: $Z(ee)H$. The bottom inset in each figure shows the ratio of the number of events observed in data to that of the Monte Carlo prediction for signal and backgrounds.

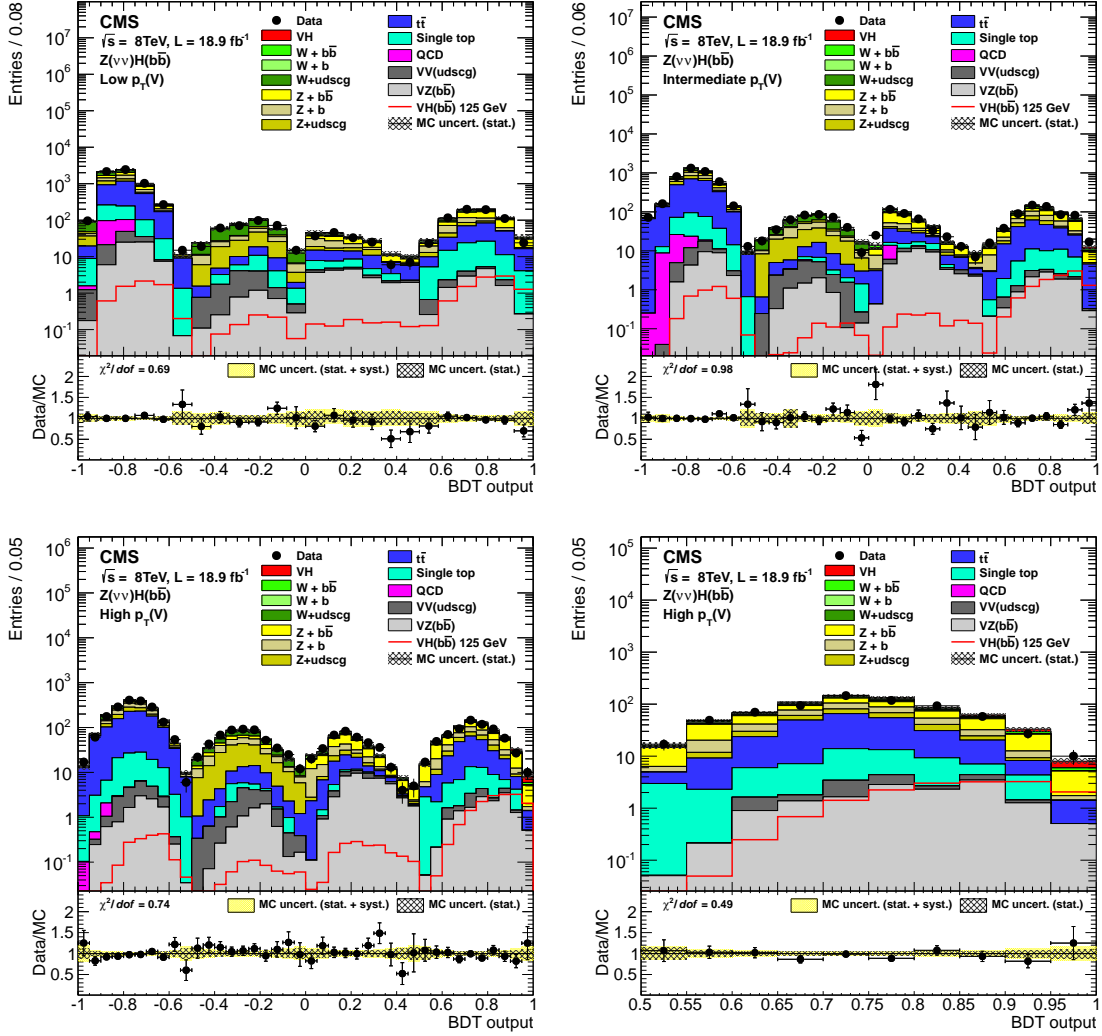


Figure 14: Post-fit BDT output distributions for $Z(\nu\nu)H$ in the low-boost region (left), the intermediate-boost (right), and the high-boost (bottom), for 8 TeV data (points with error bars), all backgrounds, and signal, after all selection criteria have been applied. Bottom right: the VH-enriched partition of the high-boost region is shown in more detail. The bottom inset in each figure shows the ratio of the number of events observed in data to that of the Monte Carlo prediction for signal and backgrounds.

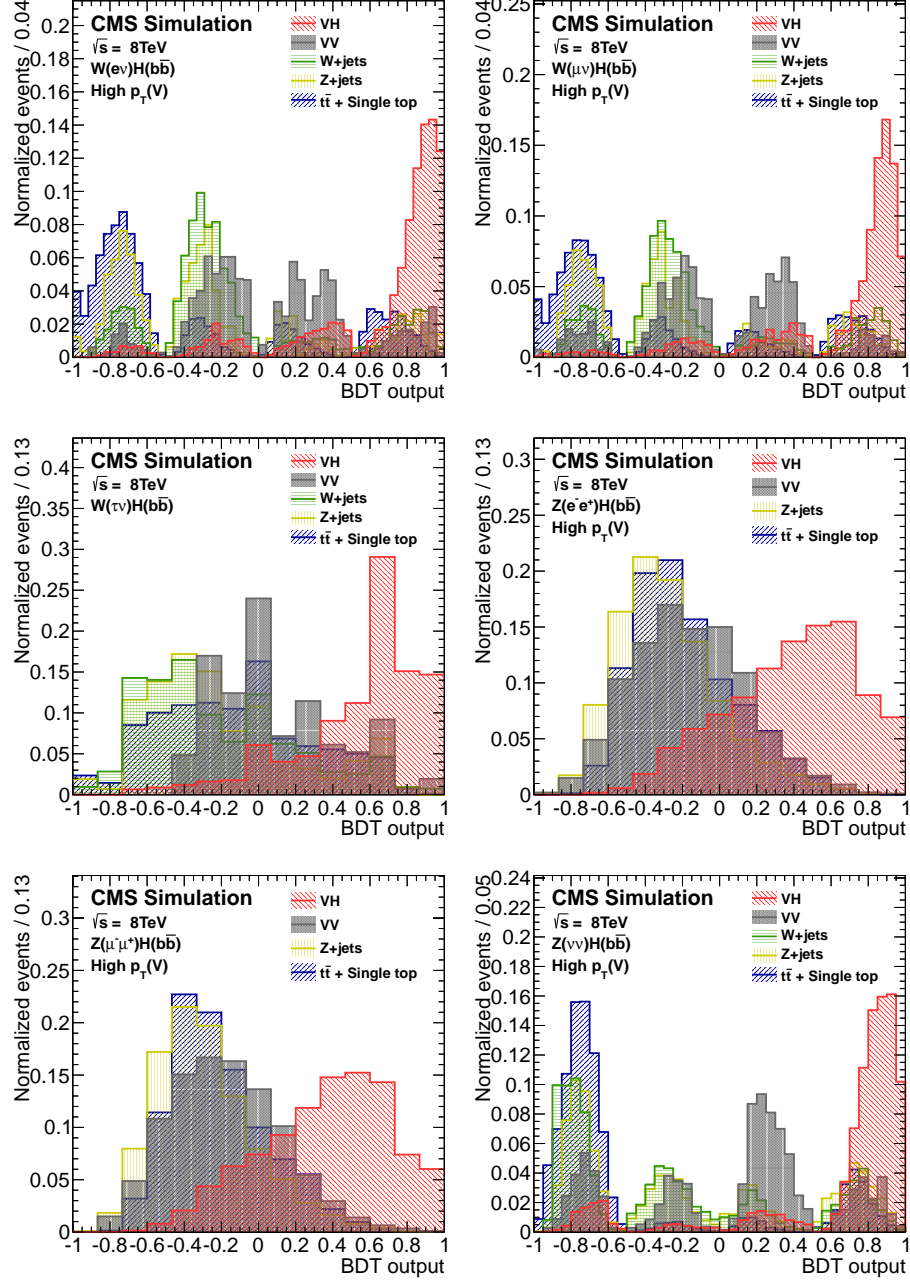


Figure 15: BDT output distributions, normalized to unity, for the highest-boost region in each channel, for all backgrounds and signal, after all selection criteria have been applied.

A The CMS Collaboration

Yerevan Physics Institute, Yerevan, Armenia

S. Chatrchyan, V. Khachatryan, A.M. Sirunyan, A. Tumasyan

Institut für Hochenergiephysik der OeAW, Wien, Austria

W. Adam, T. Bergauer, M. Dragicevic, J. Erö, C. Fabjan¹, M. Friedl, R. Frühwirth¹, V.M. Ghete, N. Hörmann, J. Hrubec, M. Jeitler¹, W. Kiesenhofer, V. Knünz, M. Krammer¹, I. Krätschmer, D. Liko, I. Mikulec, D. Rabady², B. Rahbaran, C. Rohringer, H. Rohringer, R. Schöfbeck, J. Strauss, A. Taurok, W. Treberer-Treberspurg, W. Waltenberger, C.-E. Wulz¹

National Centre for Particle and High Energy Physics, Minsk, Belarus

V. Mossolov, N. Shumeiko, J. Suarez Gonzalez

Universiteit Antwerpen, Antwerpen, Belgium

S. Alderweireldt, M. Bansal, S. Bansal, T. Cornelis, E.A. De Wolf, X. Janssen, A. Knutsson, S. Luyckx, L. Mucibello, S. Ochesanu, B. Roland, R. Rougny, Z. Staykova, H. Van Haevermaet, P. Van Mechelen, N. Van Remortel, A. Van Spilbeeck

Vrije Universiteit Brussel, Brussel, Belgium

F. Blekman, S. Blyweert, J. D'Hondt, N. Heracleous, A. Kalogeropoulos, J. Keaveney, S. Lowette, M. Maes, A. Olbrechts, S. Tavernier, W. Van Doninck, P. Van Mulders, G.P. Van Onsem, I. Villella

Université Libre de Bruxelles, Bruxelles, Belgium

C. Caillol, B. Clerbaux, G. De Lentdecker, L. Favart, A.P.R. Gay, T. Hreus, A. Léonard, P.E. Marage, A. Mohammadi, L. Perniè, T. Reis, T. Seva, L. Thomas, C. Vander Velde, P. Vanlaer, J. Wang

Ghent University, Ghent, Belgium

V. Adler, K. Beernaert, L. Benucci, A. Cimmino, S. Costantini, S. Dildick, G. Garcia, B. Klein, J. Lellouch, A. Marinov, J. McCartin, A.A. Ocampo Rios, D. Ryckbosch, M. Sigamani, N. Strobbe, F. Thyssen, M. Tytgat, S. Walsh, E. Yazgan, N. Zaganidis

Université Catholique de Louvain, Louvain-la-Neuve, Belgium

S. Basegmez, C. Beluffi³, G. Bruno, R. Castello, A. Caudron, L. Ceard, G.G. Da Silva, C. Delaere, T. du Pree, D. Favart, L. Forthomme, A. Giammanco⁴, J. Hollar, P. Jez, V. Lemaitre, J. Liao, O. Militaru, C. Nuttens, D. Pagano, A. Pin, K. Piotrkowski, A. Popov⁵, M. Selvaggi, M. Vidal Marono, J.M. Vizan Garcia

Université de Mons, Mons, Belgium

N. Beliy, T. Caebergs, E. Daubie, G.H. Hammad

Centro Brasileiro de Pesquisas Fisicas, Rio de Janeiro, Brazil

G.A. Alves, M. Correa Martins Junior, T. Martins, M.E. Pol, M.H.G. Souza

Universidade do Estado do Rio de Janeiro, Rio de Janeiro, Brazil

W.L. Aldá Júnior, W. Carvalho, J. Chinellato⁶, A. Custódio, E.M. Da Costa, D. De Jesus Damiao, C. De Oliveira Martins, S. Fonseca De Souza, H. Malbouisson, M. Malek, D. Matos Figueiredo, L. Mundim, H. Nogima, W.L. Prado Da Silva, J. Santaolalla, A. Santoro, A. Sznajder, E.J. Tonelli Manganote⁶, A. Vilela Pereira

Universidade Estadual Paulista ^a, Universidade Federal do ABC ^b, São Paulo, Brazil

C.A. Bernardes^b, F.A. Dias^{a,7}, T.R. Fernandez Perez Tomei^a, E.M. Gregores^b, C. Lagana^a, P.G. Mercadante^b, S.F. Novaes^a, Sandra S. Padula^a

Institute for Nuclear Research and Nuclear Energy, Sofia, Bulgaria

V. Genchev², P. Iaydjiev², S. Piperov, M. Rodozov, G. Sultanov, M. Vutova

University of Sofia, Sofia, Bulgaria

A. Dimitrov, I. Glushkov, R. Hadjiiska, V. Kozhuharov, L. Litov, B. Pavlov, P. Petkov

Institute of High Energy Physics, Beijing, China

J.G. Bian, G.M. Chen, H.S. Chen, C.H. Jiang, D. Liang, S. Liang, X. Meng, J. Tao, X. Wang, Z. Wang

State Key Laboratory of Nuclear Physics and Technology, Peking University, Beijing, China

C. Asawatangtrakuldee, Y. Ban, Y. Guo, Q. Li, W. Li, S. Liu, Y. Mao, S.J. Qian, D. Wang, L. Zhang, W. Zou

Universidad de Los Andes, Bogota, Colombia

C. Avila, C.A. Carrillo Montoya, L.F. Chaparro Sierra, J.P. Gomez, B. Gomez Moreno, J.C. Sanabria

Technical University of Split, Split, Croatia

N. Godinovic, D. Lelas, R. Plestina⁸, D. Polic, I. Puljak

University of Split, Split, Croatia

Z. Antunovic, M. Kovac

Institute Rudjer Boskovic, Zagreb, Croatia

V. Brigljevic, K. Kadija, J. Luetic, D. Mekterovic, S. Morovic, L. Tikvica

University of Cyprus, Nicosia, Cyprus

A. Attikis, G. Mavromanolakis, J. Mousa, C. Nicolaou, F. Ptochos, P.A. Razis

Charles University, Prague, Czech Republic

M. Finger, M. Finger Jr.

Academy of Scientific Research and Technology of the Arab Republic of Egypt, Egyptian Network of High Energy Physics, Cairo, Egypt

A.A. Abdelalim⁹, Y. Assran¹⁰, S. Elgammal⁹, A. Ellithi Kamel¹¹, M.A. Mahmoud¹², A. Radi^{13,14}

National Institute of Chemical Physics and Biophysics, Tallinn, Estonia

M. Kadastik, M. Müntel, M. Murumaa, M. Raidal, L. Rebane, A. Tiko

Department of Physics, University of Helsinki, Helsinki, Finland

P. Eerola, G. Fedi, M. Voutilainen

Helsinki Institute of Physics, Helsinki, Finland

J. Härkönen, V. Karimäki, R. Kinnunen, M.J. Kortelainen, T. Lampén, K. Lassila-Perini, S. Lehti, T. Lindén, P. Luukka, T. Mäenpää, T. Peltola, E. Tuominen, J. Tuominiemi, E. Tuovinen, L. Wendland

Lappeenranta University of Technology, Lappeenranta, Finland

T. Tuuva

DSM/IRFU, CEA/Saclay, Gif-sur-Yvette, France

M. Besancon, F. Couderc, M. Dejardin, D. Denegri, B. Fabbro, J.L. Faure, F. Ferri, S. Ganjour, A. Givernaud, P. Gras, G. Hamel de Monchenault, P. Jarry, E. Locci, J. Malcles, A. Nayak, J. Rander, A. Rosowsky, M. Titov

Laboratoire Leprince-Ringuet, Ecole Polytechnique, IN2P3-CNRS, Palaiseau, France

S. Baffioni, F. Beaudette, L. Benhabib, M. Bluj¹⁵, P. Busson, C. Charlot, N. Daci, T. Dahms, M. Dalchenko, L. Dobrzynski, A. Florent, R. Granier de Cassagnac, M. Haguénauer, P. Miné, C. Mironov, I.N. Naranjo, M. Nguyen, C. Ochando, P. Paganini, D. Sabes, R. Salerno, Y. Sirois, C. Veelken, A. Zabi

Institut Pluridisciplinaire Hubert Curien, Université de Strasbourg, Université de Haute Alsace Mulhouse, CNRS/IN2P3, Strasbourg, France

J.-L. Agram¹⁶, J. Andrea, D. Bloch, J.-M. Brom, E.C. Chabert, C. Collard,

E. Conte¹⁶, F. Drouhin¹⁶, J.-C. Fontaine¹⁶, D. Gelé, U. Goerlach, C. Goetzmann, P. Juillot, A.-C. Le Bihan, P. Van Hove

Centre de Calcul de l'Institut National de Physique Nucleaire et de Physique des Particules, CNRS/IN2P3, Villeurbanne, France

S. Gadrat

Université de Lyon, Université Claude Bernard Lyon 1, CNRS-IN2P3, Institut de Physique Nucléaire de Lyon, Villeurbanne, France

S. Beauceron, N. Beaupere, G. Boudoul, S. Brochet, J. Chasserat, R. Chierici, D. Contardo, P. Depasse, H. El Mamouni, J. Fan, J. Fay, S. Gascon, M. Gouzevitch, B. Ille, T. Kurca, M. Lethuillier, L. Mirabito, S. Perries, J.D. Ruiz Alvarez¹⁷, L. Sgandurra, V. Sordini, M. Vander Donckt, P. Verdier, S. Viret, H. Xiao

Institute of High Energy Physics and Informatization, Tbilisi State University, Tbilisi, Georgia

Z. Tsamalaidze¹⁸

RWTH Aachen University, I. Physikalisches Institut, Aachen, Germany

C. Autermann, S. Beranek, M. Bontenackels, B. Calpas, M. Edelhoff, L. Feld, O. Hindrichs, K. Klein, A. Ostapchuk, A. Perieanu, F. Raupach, J. Sammet, S. Schael, D. Sprenger, H. Weber, B. Wittmer, V. Zhukov⁵

RWTH Aachen University, III. Physikalisches Institut A, Aachen, Germany

M. Ata, J. Caudron, E. Dietz-Laursonn, D. Duchardt, M. Erdmann, R. Fischer, A. Güth, T. Hebbeker, C. Heidemann, K. Hoepfner, D. Klingebiel, S. Knutzen, P. Kreuzer, M. Merschmeyer, A. Meyer, M. Olschewski, K. Padeken, P. Papacz, H. Pieta, H. Reithler, S.A. Schmitz, L. Sonnenschein, J. Steggemann, D. Teyssier, S. Thüer, M. Weber

RWTH Aachen University, III. Physikalisches Institut B, Aachen, Germany

V. Cherepanov, Y. Erdogan, G. Flügge, H. Geenen, M. Geisler, W. Haj Ahmad, F. Hoehle, B. Kargoll, T. Kress, Y. Kuessel, J. Lingemann², A. Nowack, I.M. Nugent, L. Perchalla, O. Pooth, A. Stahl

Deutsches Elektronen-Synchrotron, Hamburg, Germany

I. Asin, N. Bartosik, J. Behr, W. Behrenhoff, U. Behrens, A.J. Bell, M. Bergholz¹⁹, A. Bethani, K. Borras, A. Burgmeier, A. Cakir, L. Calligaris, A. Campbell, S. Choudhury, F. Costanza, C. Diez Pardos, S. Dooling, T. Dorland, G. Eckerlin, D. Eckstein, G. Flucke, A. Geiser, A. Grebenyuk, P. Gunnellini, S. Habib, J. Hauk, G. Hellwig, D. Horton, H. Jung, M. Kasemann, P. Katsas, C. Kleinwort, H. Kluge, M. Krämer, D. Krücker, W. Lange, J. Leonard, K. Lipka, W. Lohmann¹⁹,

B. Lutz, R. Mankel, I. Marfin, I.-A. Melzer-Pellmann, A.B. Meyer, J. Mnich, A. Mussgiller, S. Naumann-Emme, O. Novgorodova, F. Nowak, J. Olzem, H. Perrey, A. Petrukhin, D. Pitzl, R. Placakyte, A. Raspereza, P.M. Ribeiro Cipriano, C. Riedl, E. Ron, M.Ö. Sahin, J. Salfeld-Nebgen, R. Schmidt¹⁹, T. Schoerner-Sadenius, N. Sen, M. Stein, R. Walsh, C. Wissing

University of Hamburg, Hamburg, Germany

M. Aldaya Martin, V. Blobel, H. Enderle, J. Erfle, E. Garutti, U. Gebbert, M. Görner, M. Gosselink, J. Haller, K. Heine, R.S. Höing, G. Kaussen, H. Kirschenmann, R. Klanner, R. Kogler, J. Lange, I. Marchesini, T. Peiffer, N. Pietsch, D. Rathjens, C. Sander, H. Schettler, P. Schleper, E. Schlieckau, A. Schmidt, M. Schröder, T. Schum, M. Seidel, J. Sibille²⁰, V. Sola, H. Stadie, G. Steinbrück, J. Thomsen, D. Troendle, E. Usai, L. Vanelderen

Institut für Experimentelle Kernphysik, Karlsruhe, Germany

C. Barth, C. Baus, J. Berger, C. Böser, E. Butz, T. Chwalek, W. De Boer, A. Descroix, A. Dierlamm, M. Feindt, M. Guthoff², F. Hartmann², T. Hauth², H. Held, K.H. Hoffmann, U. Husemann, I. Katkov⁵, J.R. Komaragiri, A. Kornmayer², E. Kuznetsova, P. Lobelle Pardo, D. Martschei, M.U. Mozer, Th. Müller, M. Niegel, A. Nürnberg, O. Oberst, J. Ott, G. Quast, K. Rabbertz, F. Ratnikov, S. Röcker, F.-P. Schilling, G. Schott, H.J. Simonis, F.M. Stober, R. Ulrich, J. Wagner-Kuhr, S. Wayand, T. Weiler, M. Zeise

Institute of Nuclear and Particle Physics (INPP), NCSR Demokritos, Aghia Paraskevi, Greece

G. Anagnostou, G. Daskalakis, T. Geralis, S. Kesisoglou, A. Kyriakis, D. Loukas, A. Markou, C. Markou, E. Ntomari, I. Topsis-giotis

University of Athens, Athens, Greece

L. Gouskos, A. Panagiotou, N. Saoulidou, E. Stiliaris

University of Ioánnina, Ioánnina, Greece

X. Aslanoglou, I. Evangelou, G. Flouris, C. Foudas, P. Kokkas, N. Manthos, I. Papadopoulos, E. Paradas

KFKI Research Institute for Particle and Nuclear Physics, Budapest, Hungary

G. Bencze, C. Hajdu, P. Hidas, D. Horvath²¹, F. Sikler, V. Veszpremi, G. Vesztergombi²², A.J. Zsigmond

Institute of Nuclear Research ATOMKI, Debrecen, Hungary

N. Beni, S. Czellar, J. Molnar, J. Palinkas, Z. Szillasi

University of Debrecen, Debrecen, Hungary

J. Karancsi, P. Raics, Z.L. Trocsanyi, B. Ujvari

National Institute of Science Education and Research, Bhubaneswar, India

S.K. Swain²³

Panjab University, Chandigarh, India

S.B. Beri, V. Bhatnagar, N. Dhingra, R. Gupta, M. Kaur, M.Z. Mehta, M. Mittal, N. Nishu, A. Sharma, J.B. Singh

University of Delhi, Delhi, India

Ashok Kumar, Arun Kumar, S. Ahuja, A. Bhardwaj, B.C. Choudhary, A. Kumar, S. Malhotra, M. Naimuddin, K. Ranjan, P. Saxena, V. Sharma, R.K. Shivpuri

Saha Institute of Nuclear Physics, Kolkata, India

S. Banerjee, S. Bhattacharya, K. Chatterjee, S. Dutta, B. Gomber, Sa. Jain, Sh. Jain, R. Khurana, A. Modak, S. Mukherjee, D. Roy, S. Sarkar, M. Sharan, A.P. Singh

Bhabha Atomic Research Centre, Mumbai, India

A. Abdulsalam, D. Dutta, S. Kailas, V. Kumar, A.K. Mohanty², L.M. Pant, P. Shukla, A. Topkar

Tata Institute of Fundamental Research - EHEP, Mumbai, India

T. Aziz, R.M. Chatterjee, S. Ganguly, S. Ghosh, M. Guchait²⁴, A. Gurtu²⁵, G. Kole, S. Kumar, M. Maity²⁶, G. Majumder, K. Mazumdar, G.B. Mohanty, B. Parida, K. Sudhakar, N. Wickramage²⁷

Tata Institute of Fundamental Research - HECR, Mumbai, India

S. Banerjee, S. Dugad

Institute for Research in Fundamental Sciences (IPM), Tehran, Iran

H. Arfaei, H. Bakhshiansohi, S.M. Etesami²⁸, A. Fahim²⁹, A. Jafari, M. Khakzad, M. Mohammadi Najafabadi, S. Paktinat Mehdiabadi, B. Safarzadeh³⁰, M. Zeinali

University College Dublin, Dublin, Ireland

M. Grunewald

INFN Sezione di Bari ^a, Università di Bari ^b, Politecnico di Bari ^c, Bari, Italy

M. Abbrescia^{a,b}, L. Barbone^{a,b}, C. Calabria^{a,b}, S.S. Chhibra^{a,b}, A. Colaleo^a, D. Creanza^{a,c}, N. De Filippis^{a,c}, M. De Palma^{a,b}, L. Fiore^a, G. Iaselli^{a,c}, G. Maggi^{a,c}, M. Maggi^a, B. Marangelli^{a,b}, S. My^{a,c}, S. Nuzzo^{a,b}, N. Pacifico^a, A. Pompili^{a,b}, G. Pugliese^{a,c}, R. Radogna^{a,b}, G. Selvaggi^{a,b}, L. Silvestris^a, G. Singh^{a,b}, R. Venditti^{a,b}, P. Verwilligen^a, G. Zito^a

INFN Sezione di Bologna ^a, Università di Bologna ^b, Bologna, Italy

G. Abbiendi^a, A.C. Benvenuti^a, D. Bonacorsi^{a,b}, S. Braibant-Giacomelli^{a,b},
 L. Brigliadori^{a,b}, R. Campanini^{a,b}, P. Capiluppi^{a,b}, A. Castro^{a,b}, F.R. Cavallo^a,
 G. Codispoti^{a,b}, M. Cuffiani^{a,b}, G.M. Dallavalle^a, F. Fabbri^a, A. Fanfani^{a,b},
 D. Fasanella^{a,b}, P. Giacomelli^a, C. Grandi^a, L. Guiducci^{a,b}, S. Marcellini^a,
 G. Masetti^a, M. Meneghelli^{a,b}, A. Montanari^a, F.L. Navarria^{a,b}, F. Odorici^a,
 A. Perrotta^a, F. Primavera^{a,b}, A.M. Rossi^{a,b}, T. Rovelli^{a,b}, G.P. Siroli^{a,b}, N. Tosi^{a,b},
 R. Travaglini^{a,b}

INFN Sezione di Catania ^a, Università di Catania ^b, Catania, Italy

S. Albergo^{a,b}, G. Cappello^a, M. Chiorboli^{a,b}, S. Costa^{a,b}, F. Giordano^{a,2},
 R. Potenza^{a,b}, A. Tricomi^{a,b}, C. Tuve^{a,b}

INFN Sezione di Firenze ^a, Università di Firenze ^b, Firenze, Italy

G. Barbagli^a, V. Ciulli^{a,b}, C. Civinini^a, R. D'Alessandro^{a,b}, E. Focardi^{a,b},
 S. Frosali^{a,b}, E. Gallo^a, S. Gonzi^{a,b}, V. Gori^{a,b}, P. Lenzi^{a,b}, M. Meschini^a,
 S. Paoletti^a, G. Sguazzoni^a, A. Tropiano^{a,b}

INFN Laboratori Nazionali di Frascati, Frascati, Italy

L. Benussi, S. Bianco, F. Fabbri, D. Piccolo

INFN Sezione di Genova ^a, Università di Genova ^b, Genova, Italy

P. Fabbriatore^a, R. Ferretti^{a,b}, F. Ferro^a, M. Lo Vetere^{a,b}, R. Musenich^a,
 E. Robutti^a, S. Tosi^{a,b}

INFN Sezione di Milano-Bicocca ^a, Università di Milano-Bicocca ^b, Milano, Italy

A. Benaglia^a, M.E. Dinardo^{a,b}, S. Fiorendi^{a,b}, S. Gennai^a, A. Ghezzi^{a,b},
 P. Govoni^{a,b}, M.T. Lucchini^{a,b,2}, S. Malvezzi^a, R.A. Manzoni^{a,b,2}, A. Martelli^{a,b,2},
 D. Menasce^a, L. Moroni^a, M. Paganoni^{a,b}, D. Pedrini^a, S. Ragazzi^{a,b}, N. Redaelli^a,
 T. Tabarelli de Fatis^{a,b}

INFN Sezione di Napoli ^a, Università di Napoli 'Federico II' ^b, Università della Basilicata (Potenza) ^c, Università G. Marconi (Roma) ^d, Napoli, Italy

S. Buontempo^a, N. Cavallo^{a,c}, F. Fabozzi^{a,c}, A.O.M. Iorio^{a,b}, L. Lista^a,
 S. Meola^{a,d,2}, M. Merola^a, P. Paolucci^{a,2}

INFN Sezione di Padova ^a, Università di Padova ^b, Università di Trento (Trento) ^c, Padova, Italy

P. Azzi^a, N. Bacchetta^a, D. Bisello^{a,b}, A. Branca^{a,b}, R. Carlin^{a,b}, P. Checchia^a,
 T. Dorigo^a, U. Dosselli^a, F. Fanzago^a, M. Galanti^{a,b,2}, F. Gasparini^{a,b},
 U. Gasparini^{a,b}, P. Giubilato^{a,b}, F. Gonella^a, A. Gozzelino^a, K. Kanishchev^{a,c},

S. Lacaprara^a, I. Lazzizzera^{a,c}, M. Margoni^{a,b}, A.T. Meneguzzo^{a,b}, J. Pazzini^{a,b},
N. Pozzobon^{a,b}, P. Ronchese^{a,b}, F. Simonetto^{a,b}, E. Torassa^a, M. Tosi^{a,b},
S. Vanini^{a,b}, P. Zotto^{a,b}, A. Zucchetta^{a,b}, G. Zumerle^{a,b}

INFN Sezione di Pavia^a, Università di Pavia^b, Pavia, Italy

M. Gabusi^{a,b}, S.P. Ratti^{a,b}, C. Riccardi^{a,b}, P. Vitulo^{a,b}

INFN Sezione di Perugia^a, Università di Perugia^b, Perugia, Italy

M. Biasini^{a,b}, G.M. Bilei^a, L. Fanò^{a,b}, P. Lariccia^{a,b}, G. Mantovani^{a,b},
M. Menichelli^a, A. Nappi^{a,b†}, F. Romeo^{a,b}, A. Saha^a, A. Santocchia^{a,b}, A. Spiezia^{a,b}

INFN Sezione di Pisa^a, Università di Pisa^b, Scuola Normale Superiore di Pisa^c, Pisa, Italy

K. Androsov^{a,31}, P. Azzurri^a, G. Bagliesi^a, J. Bernardini^a, T. Boccali^a,
G. Broccolo^{a,c}, R. Castaldi^a, M.A. Ciocci^{a,31}, R. Dell'Orso^a, S. Donato^{a,c},
F. Fiori^{a,c}, L. Foà^{a,c}, A. Giassi^a, M.T. Grippo^{a,31}, A. Kraan^a, F. Ligabue^{a,c},
T. Lomtadze^a, L. Martini^{a,b}, A. Messineo^{a,b}, C.S. Moon^{a,32}, F. Palla^a, A. Rizzi^{a,b},
A. Savoy-Navarro^{a,33}, A.T. Serban^a, P. Spagnolo^a, P. Squillacioti^{a,31}, R. Tenchini^a,
G. Tonelli^{a,b}, A. Venturi^a, P.G. Verdini^a, C. Vernieri^{a,c}

INFN Sezione di Roma^a, Università di Roma^b, Roma, Italy

L. Barone^{a,b}, F. Cavallari^a, D. Del Re^{a,b}, M. Diemoz^a, M. Grassi^{a,b}, C. Jorda^a,
E. Longo^{a,b}, F. Margaroli^{a,b}, P. Meridiani^a, F. Micheli^{a,b}, S. Nourbakhsh^{a,b},
G. Organtini^{a,b}, R. Paramatti^a, S. Rahatlou^{a,b}, C. Rovelli^a, L. Soffi^{a,b}

INFN Sezione di Torino^a, Università di Torino^b, Università del Piemonte Orientale (Novara)^c, Torino, Italy

N. Amapane^{a,b}, R. Arcidiacono^{a,c}, S. Argiro^{a,b}, M. Arneodo^{a,c}, R. Bellan^{a,b},
C. Biino^a, N. Cartiglia^a, S. Casasso^{a,b}, M. Costa^{a,b}, A. Degano^{a,b}, N. Demaria^a,
C. Mariotti^a, S. Maselli^a, E. Migliore^{a,b}, V. Monaco^{a,b}, M. Musich^a,
M.M. Obertino^{a,c}, N. Pastrone^a, M. Pelliccioni^{a,2}, A. Potenza^{a,b}, A. Romero^{a,b},
M. Ruspa^{a,c}, R. Sacchi^{a,b}, A. Solano^{a,b}, A. Staiano^a, U. Tamponi^a

INFN Sezione di Trieste^a, Università di Trieste^b, Trieste, Italy

S. Belforte^a, V. Candelise^{a,b}, M. Casarsa^a, F. Cossutti^{a,2}, G. Della Ricca^{a,b},
B. Gobbo^a, C. La Licata^{a,b}, M. Marone^{a,b}, D. Montanino^{a,b}, A. Penzo^a,
A. Schizzi^{a,b}, T. Umer^{a,b}, A. Zanetti^a

Kangwon National University, Chunchon, Korea

S. Chang, T.Y. Kim, S.K. Nam

Kyungpook National University, Daegu, Korea

D.H. Kim, G.N. Kim, J.E. Kim, D.J. Kong, S. Lee, Y.D. Oh, H. Park, D.C. Son

Chonnam National University, Institute for Universe and Elementary Particles, Kwangju, Korea

J.Y. Kim, Zero J. Kim, S. Song

Korea University, Seoul, Korea

S. Choi, D. Gyun, B. Hong, M. Jo, H. Kim, T.J. Kim, K.S. Lee, S.K. Park, Y. Roh

University of Seoul, Seoul, Korea

M. Choi, J.H. Kim, C. Park, I.C. Park, S. Park, G. Ryu

Sungkyunkwan University, Suwon, Korea

Y. Choi, Y.K. Choi, J. Goh, M.S. Kim, E. Kwon, B. Lee, J. Lee, S. Lee, H. Seo, I. Yu

Vilnius University, Vilnius, Lithuania

I. Grigelionis, A. Juodagalvis

Centro de Investigacion y de Estudios Avanzados del IPN, Mexico City, Mexico

H. Castilla-Valdez, E. De La Cruz-Burelo, I. Heredia-de La Cruz³⁴, R. Lopez-Fernandez, J. Martínez-Ortega, A. Sanchez-Hernandez, L.M. Villaseñor-Cendejas

Universidad Iberoamericana, Mexico City, Mexico

S. Carrillo Moreno, F. Vazquez Valencia

Benemerita Universidad Autonoma de Puebla, Puebla, Mexico

H.A. Salazar Ibarguen

Universidad Autónoma de San Luis Potosí, San Luis Potosí, Mexico

E. Casimiro Linares, A. Morelos Pineda, M.A. Reyes-Santos

University of Auckland, Auckland, New Zealand

D. Krofcheck

University of Canterbury, Christchurch, New Zealand

P.H. Butler, R. Doesburg, S. Reucroft, H. Silverwood

National Centre for Physics, Quaid-I-Azam University, Islamabad, Pakistan

M. Ahmad, M.I. Asghar, J. Butt, H.R. Hoorani, S. Khalid, W.A. Khan, T. Khurshid, S. Qazi, M.A. Shah, M. Shoaib

National Centre for Nuclear Research, Swierk, Poland

H. Bialkowska, B. Boimska, T. Frueboes, M. Górski, M. Kazana, K. Nawrocki, K. Romanowska-Rybinska, M. Szleper, G. Wrochna, P. Zalewski

Institute of Experimental Physics, Faculty of Physics, University of Warsaw, Warsaw, Poland

G. Brona, K. Bunkowski, M. Cwiok, W. Dominik, K. Doroba, A. Kalinowski, M. Konecki, J. Krolikowski, M. Misiura, W. Wolszczak

Laboratório de Instrumentação e Física Experimental de Partículas, Lisboa, Portugal

N. Almeida, P. Bargassa, C. Beirão Da Cruz E Silva, P. Faccioli, P.G. Ferreira Parracho, M. Gallinaro, F. Nguyen, J. Rodrigues Antunes, J. Seixas², J. Varela, P. Vischia

Joint Institute for Nuclear Research, Dubna, Russia

S. Afanasiev, P. Bunin, M. Gavrilenko, I. Golutvin, I. Gorbunov, A. Kamenev, V. Karjavin, V. Konoplyanikov, A. Lanev, A. Malakhov, V. Matveev, P. Moisezenz, V. Palichik, V. Perelygin, S. Shmatov, N. Skatchkov, V. Smirnov, A. Zarubin

Petersburg Nuclear Physics Institute, Gatchina (St. Petersburg), Russia

S. Evstyukhin, V. Golovtsov, Y. Ivanov, V. Kim, P. Levchenko, V. Murzin, V. Oreshkin, I. Smirnov, V. Sulimov, L. Uvarov, S. Vavilov, A. Vorobyev, An. Vorobyev

Institute for Nuclear Research, Moscow, Russia

Yu. Andreev, A. Dermenev, S. Gninenko, N. Golubev, M. Kirsanov, N. Krasnikov, A. Pashenkov, D. Tlisov, A. Toropin

Institute for Theoretical and Experimental Physics, Moscow, Russia

V. Epshteyn, V. Gavrilov, N. Lychkovskaya, V. Popov, G. Safronov, S. Semenov, A. Spiridonov, V. Stolin, E. Vlasov, A. Zhokin

P.N. Lebedev Physical Institute, Moscow, Russia

V. Andreev, M. Azarkin, I. Dremin, M. Kirakosyan, A. Leonidov, G. Mesyats, S.V. Rusakov, A. Vinogradov

Skobeltsyn Institute of Nuclear Physics, Lomonosov Moscow State University, Moscow, Russia

A. Belyaev, E. Boos, V. Bunichev, M. Dubinin⁷, L. Dudko, A. Ershov, A. Kaminskiy³⁵, V. Klyukhin, O. Kodolova, I. Lokhtin, A. Markina, S. Obraztsov, S. Petrushanko, V. Savrin

State Research Center of Russian Federation, Institute for High Energy Physics, Protvino, Russia

I. Azhgirey, I. Bayshev, S. Bitioukov, V. Kachanov, A. Kalinin, D. Konstantinov,

V. Krychkine, V. Petrov, R. Ryutin, A. Sobol, L. Tourtchanovitch, S. Troshin, N. Tyurin, A. Uzunian, A. Volkov

University of Belgrade, Faculty of Physics and Vinca Institute of Nuclear Sciences, Belgrade, Serbia

P. Adzic³⁶, M. Djordjevic, M. Ekmedzic, J. Milosevic

Centro de Investigaciones Energéticas Medioambientales y Tecnológicas (CIEMAT), Madrid, Spain

M. Aguilar-Benitez, J. Alcaraz Maestre, C. Battilana, E. Calvo, M. Cerrada, M. Chamizo Llatas², N. Colino, B. De La Cruz, A. Delgado Peris, D. Domínguez Vázquez, C. Fernandez Bedoya, J.P. Fernández Ramos, A. Ferrando, J. Flix, M.C. Fouz, P. Garcia-Abia, O. Gonzalez Lopez, S. Goy Lopez, J.M. Hernandez, M.I. Josa, G. Merino, E. Navarro De Martino, J. Puerta Pelayo, A. Quintario Olmeda, I. Redondo, L. Romero, M.S. Soares, C. Willmott

Universidad Autónoma de Madrid, Madrid, Spain

C. Albajar, J.F. de Trocóniz

Universidad de Oviedo, Oviedo, Spain

H. Brun, J. Cuevas, J. Fernandez Menendez, S. Folgueras, I. Gonzalez Caballero, L. Lloret Iglesias

Instituto de Física de Cantabria (IFCA), CSIC-Universidad de Cantabria, Santander, Spain

J.A. Brochero Cifuentes, I.J. Cabrillo, A. Calderon, S.H. Chuang, J. Duarte Campderros, M. Fernandez, G. Gomez, J. Gonzalez Sanchez, A. Graziano, A. Lopez Virto, J. Marco, R. Marco, C. Martinez Rivero, F. Matorras, F.J. Munoz Sanchez, J. Piedra Gomez, T. Rodrigo, A.Y. Rodríguez-Marrero, A. Ruiz-Jimeno, L. Scodellaro, I. Vila, R. Vilar Cortabitarte

CERN, European Organization for Nuclear Research, Geneva, Switzerland

D. Abbaneo, E. Auffray, G. Auzinger, M. Bachtis, P. Baillon, A.H. Ball, D. Barney, J. Bendavid, J.F. Benitez, C. Bernet⁸, G. Bianchi, P. Bloch, A. Bocci, A. Bonato, O. Bondu, C. Botta, H. Breuker, T. Camporesi, G. Cerminara, T. Christiansen, J.A. Coarasa Perez, S. Colafranceschi³⁷, M. D'Alfonso, D. d'Enterria, A. Dabrowski, A. David, F. De Guio, A. De Roeck, S. De Visscher, S. Di Guida, M. Dobson, N. Dupont-Sagorin, A. Elliott-Peisert, J. Eugster, G. Franzoni, W. Funk, M. Giffels, D. Gigi, K. Gill, D. Giordano, M. Girone, M. Giunta, F. Glege, R. Gomez-Reino Garrido, S. Gowdy, R. Guida, J. Hammer, M. Hansen, P. Harris, C. Hartl, A. Hinemann, V. Innocente, P. Janot, E. Karavakis,

K. Kousouris, K. Krajczar, P. Lecoq, Y.-J. Lee, C. Lourenço, N. Magini, L. Malgeri, M. Mannelli, L. Masetti, F. Meijers, S. Mersi, E. Meschi, M. Mulders, P. Musella, L. Orsini, E. Palencia Cortezon, E. Perez, L. Perrozzi, A. Petrilli, G. Petrucciani, A. Pfeiffer, M. Pierini, M. Pimiä, D. Piparo, M. Plagge, L. Quertenmont, A. Racz, W. Reece, G. Rolandi³⁸, M. Rovere, H. Sakulin, F. Santanastasio, C. Schäfer, C. Schwick, S. Sekmen, A. Sharma, P. Siegrist, P. Silva, M. Simon, P. Sphicas³⁹, D. Spiga, B. Stieger, M. Stoye, A. Tsirou, G.I. Veres²², J.R. Vlimant, H.K. Wöhri, W.D. Zeuner

Paul Scherrer Institut, Villigen, Switzerland

W. Bertl, K. Deiters, W. Erdmann, K. Gabathuler, R. Horisberger, Q. Ingram, H.C. Kaestli, S. König, D. Kotlinski, U. Langenegger, D. Renker, T. Rohe

Institute for Particle Physics, ETH Zurich, Zurich, Switzerland

F. Bachmair, L. Bäni, L. Bianchini, P. Bortignon, M.A. Buchmann, B. Casal, N. Chanon, A. Deisher, G. Dissertori, M. Dittmar, M. Donegà, M. Dünser, P. Eller, K. Freudenreich, C. Grab, D. Hits, P. Lecomte, W. Lustermann, B. Mangano, A.C. Marini, P. Martinez Ruiz del Arbol, D. Meister, N. Mohr, F. Moortgat, C. Nägeli⁴⁰, P. Nef, F. Nessi-Tedaldi, F. Pandolfi, L. Pape, F. Pauss, M. Peruzzi, M. Quittnat, F.J. Ronga, M. Rossini, L. Sala, A.K. Sanchez, A. Starodumov⁴¹, M. Takahashi, L. Tauscher[†], A. Thea, K. Theofilatos, D. Treille, R. Wallny, H.A. Weber

Universität Zürich, Zurich, Switzerland

C. Amsler⁴², V. Chiochia, A. De Cosa, C. Favaro, M. Ivova Rikova, B. Kilminster, B. Millan Mejias, J. Ngadiuba, P. Robmann, H. Snoek, S. Taroni, M. Verzetti, Y. Yang

National Central University, Chung-Li, Taiwan

M. Cardaci, K.H. Chen, C. Ferro, C.M. Kuo, S.W. Li, W. Lin, Y.J. Lu, R. Volpe, S.S. Yu

National Taiwan University (NTU), Taipei, Taiwan

P. Bartalini, P. Chang, Y.H. Chang, Y.W. Chang, Y. Chao, K.F. Chen, C. Dietz, U. Grundler, W.-S. Hou, Y. Hsiung, K.Y. Kao, Y.J. Lei, Y.F. Liu, R.-S. Lu, D. Majumder, E. Petrakou, X. Shi, J.G. Shiu, Y.M. Tzeng, M. Wang

Chulalongkorn University, Bangkok, Thailand

B. Asavapibhop, N. Suwonjandee

Cukurova University, Adana, Turkey

A. Adiguzel, M.N. Bakirci⁴³, S. Cerci⁴⁴, C. Dozen, I. Dumanoglu, E. Eskut,

S. Girgis, G. Gokbulut, E. Gurpinar, I. Hos, E.E. Kangal, A. Kayis Topaksu, G. Onengut⁴⁵, K. Ozdemir, S. Ozturk⁴³, A. Polatoz, K. Sogut⁴⁶, D. Sunar Cerci⁴⁴, B. Tali⁴⁴, H. Topakli⁴³, M. Vergili

Middle East Technical University, Physics Department, Ankara, Turkey

I.V. Akin, T. Aliev, B. Bilin, S. Bilmis, M. Deniz, H. Gamsizkan, A.M. Guler, G. Karapinar⁴⁷, K. Ocalan, A. Ozpineci, M. Serin, R. Sever, U.E. Surat, M. Yalvac, M. Zeyrek

Bogazici University, Istanbul, Turkey

E. Gülmez, B. Isildak⁴⁸, M. Kaya⁴⁹, O. Kaya⁴⁹, S. Ozkorucuklu⁵⁰, N. Sonmez⁵¹

Istanbul Technical University, Istanbul, Turkey

H. Bahtiyar⁵², E. Barlas, K. Cankocak, Y.O. Günaydin⁵³, F.I. Vardarli, M. Yücel

National Scientific Center, Kharkov Institute of Physics and Technology, Kharkov, Ukraine

L. Levchuk, P. Sorokin

University of Bristol, Bristol, United Kingdom

J.J. Brooke, E. Clement, D. Cussans, H. Flacher, R. Frazier, J. Goldstein, M. Grimes, G.P. Heath, H.F. Heath, J. Jacob, L. Kreczko, C. Lucas, Z. Meng, S. Metson, D.M. Newbold⁵⁴, K. Nirunpong, S. Paramesvaran, A. Poll, S. Senkin, V.J. Smith, T. Williams

Rutherford Appleton Laboratory, Didcot, United Kingdom

K.W. Bell, A. Belyaev⁵⁵, C. Brew, R.M. Brown, D.J.A. Cockerill, J.A. Coughlan, K. Harder, S. Harper, J. Ilic, E. Olaiya, D. Petyt, B.C. Radburn-Smith, C.H. Shepherd-Themistocleous, I.R. Tomalin, W.J. Womersley, S.D. Worm

Imperial College, London, United Kingdom

R. Bainbridge, O. Buchmuller, D. Burton, D. Colling, N. Cripps, M. Cutajar, P. Dauncey, G. Davies, M. Della Negra, W. Ferguson, J. Fulcher, D. Futyan, A. Gilbert, A. Guneratne Bryer, G. Hall, Z. Hatherell, J. Hays, G. Iles, M. Jarvis, G. Karapostoli, M. Kenzie, R. Lane, R. Lucas⁵⁴, L. Lyons, A.-M. Magnan, J. Marrouche, B. Mathias, R. Nandi, J. Nash, A. Nikitenko⁴¹, J. Pela, M. Pesaresi, K. Petridis, M. Pioppi⁵⁶, D.M. Raymond, S. Rogerson, A. Rose, C. Seez, P. Sharp[†], A. Sparrow, A. Tapper, M. Vazquez Acosta, T. Virdee, S. Wakefield, N. Wardle

Brunel University, Uxbridge, United Kingdom

M. Chadwick, J.E. Cole, P.R. Hobson, A. Khan, P. Kyberd, D. Leggat, D. Leslie, W. Martin, I.D. Reid, P. Symonds, L. Teodorescu, M. Turner

Baylor University, Waco, USA

J. Dittmann, K. Hatakeyama, A. Kasmi, H. Liu, T. Scarborough

The University of Alabama, Tuscaloosa, USA

O. Charaf, S.I. Cooper, C. Henderson, P. Rumerio

Boston University, Boston, USA

A. Avetisyan, T. Bose, C. Fantasia, A. Heister, P. Lawson, D. Lazic, J. Rohlf, D. Sperka, J. St. John, L. Sulak

Brown University, Providence, USA

J. Alimena, S. Bhattacharya, G. Christopher, D. Cutts, Z. Demiragli, A. Ferapontov, A. Garabedian, U. Heintz, S. Jabeen, G. Kukartsev, E. Laird, G. Landsberg, M. Luk, M. Narain, M. Segala, T. Sinthuprasith, T. Speer

University of California, Davis, Davis, USA

R. Breedon, G. Breto, M. Calderon De La Barca Sanchez, S. Chauhan, M. Chertok, J. Conway, R. Conway, P.T. Cox, R. Erbacher, M. Gardner, R. Houtz, W. Ko, A. Kopecky, R. Lander, T. Miceli, D. Pellett, J. Pilot, F. Ricci-Tam, B. Rutherford, M. Searle, J. Smith, M. Squires, M. Tripathi, S. Wilbur, R. Yohay

University of California, Los Angeles, USA

V. Andreev, D. Cline, R. Cousins, S. Erhan, P. Everaerts, C. Farrell, M. Felcini, J. Hauser, M. Ignatenko, C. Jarvis, G. Rakness, P. Schlein[†], E. Takasugi, P. Traczyk, V. Valuev, M. Weber

University of California, Riverside, Riverside, USA

J. Babb, R. Clare, J. Ellison, J.W. Gary, G. Hanson, J. Heilman, P. Jandir, F. Lacroix, H. Liu, O.R. Long, A. Luthra, M. Malberti, H. Nguyen, A. Shrinivas, J. Sturdy, S. Sumowidagdo, R. Wilken, S. Wimpenny

University of California, San Diego, La Jolla, USA

W. Andrews, J.G. Branson, G.B. Cerati, S. Cittolin, R.T. D'Agnolo, D. Evans, A. Holzner, R. Kelley, M. Lebourgeois, J. Letts, I. Macneill, S. Padhi, C. Palmer, M. Pieri, M. Sani, V. Sharma, S. Simon, E. Sudano, M. Tadel, Y. Tu, A. Vartak, S. Wasserbaech⁵⁷, F. Würthwein, A. Yagil, J. Yoo

University of California, Santa Barbara, Santa Barbara, USA

D. Barge, C. Campagnari, T. Danielson, K. Flowers, P. Geffert, C. George, F. Golf, J. Incandela, C. Justus, D. Kovalskyi, V. Krutelyov, R. Magaña Villalba, N. Mccoll, V. Pavlunin, J. Richman, R. Rossin, D. Stuart, W. To, C. West

California Institute of Technology, Pasadena, USA

A. Apresyan, A. Bornheim, J. Bunn, Y. Chen, E. Di Marco, J. Duarte, D. Kcira, Y. Ma, A. Mott, H.B. Newman, C. Pena, C. Rogan, M. Spiropulu, V. Timciuc, J. Veverka, R. Wilkinson, S. Xie, R.Y. Zhu

Carnegie Mellon University, Pittsburgh, USA

V. Azzolini, A. Calamba, R. Carroll, T. Ferguson, Y. Iiyama, D.W. Jang, M. Paulini, J. Russ, H. Vogel, I. Vorobiev

University of Colorado at Boulder, Boulder, USA

J.P. Cumalat, B.R. Drell, W.T. Ford, A. Gaz, E. Luiggi Lopez, U. Nauenberg, J.G. Smith, K. Stenson, K.A. Ulmer, S.R. Wagner

Cornell University, Ithaca, USA

J. Alexander, A. Chatterjee, N. Eggert, L.K. Gibbons, W. Hopkins, A. Khukhunaishvili, B. Kreis, N. Mirman, G. Nicolas Kaufman, J.R. Patterson, A. Ryd, E. Salvati, W. Sun, W.D. Teo, J. Thom, J. Thompson, J. Tucker, Y. Weng, L. Winstrom, P. Wittich

Fairfield University, Fairfield, USA

D. Winn

Fermi National Accelerator Laboratory, Batavia, USA

S. Abdullin, M. Albrow, J. Anderson, G. Apollinari, L.A.T. Bauerdick, A. Beretvas, J. Berryhill, P.C. Bhat, K. Burkett, J.N. Butler, V. Chetluru, H.W.K. Cheung, F. Chlebana, S. Cihangir, V.D. Elvira, I. Fisk, J. Freeman, Y. Gao, E. Gottschalk, L. Gray, D. Green, O. Gutsche, D. Hare, R.M. Harris, J. Hirschauer, B. Hooberman, S. Jindariani, M. Johnson, U. Joshi, K. Kaadze, B. Klima, S. Kunori, S. Kwan, J. Linacre, D. Lincoln, R. Lipton, J. Lykken, K. Maeshima, J.M. Marraffino, V.I. Martinez Outschoorn, S. Maruyama, D. Mason, P. McBride, K. Mishra, S. Mrenna, Y. Musienko⁵⁸, C. Newman-Holmes, V. O'Dell, O. Prokofyev, N. Ratnikova, E. Sexton-Kennedy, S. Sharma, W.J. Spalding, L. Spiegel, L. Taylor, S. Tkaczyk, N.V. Tran, L. Uplegger, E.W. Vaandering, R. Vidal, J. Whitmore, W. Wu, F. Yang, J.C. Yun

University of Florida, Gainesville, USA

D. Acosta, P. Avery, D. Bourilkov, M. Chen, T. Cheng, S. Das, M. De Gruttola, G.P. Di Giovanni, D. Dobur, A. Drozdetskiy, R.D. Field, M. Fisher, Y. Fu, I.K. Furic, J. Hugon, B. Kim, J. Konigsberg, A. Korytov, A. Kropivnitskaya, T. Kypreos, J.F. Low, K. Matchev, P. Milenovic⁵⁹, G. Mitselmakher, L. Muniz, A. Rinkevicius, N. Skhirtladze, M. Snowball, J. Yelton, M. Zakaria

Florida International University, Miami, USA

V. Gaultney, S. Hewamanage, S. Linn, P. Markowitz, G. Martinez, J.L. Rodriguez

Florida State University, Tallahassee, USA

T. Adams, A. Askew, J. Bochenek, J. Chen, B. Diamond, J. Haas, S. Hagopian, V. Hagopian, K.F. Johnson, H. Prosper, V. Veeraraghavan, M. Weinberg

Florida Institute of Technology, Melbourne, USA

M.M. Baarmand, B. Dorney, M. Hohlmann, H. Kalakhety, F. Yumiceva

University of Illinois at Chicago (UIC), Chicago, USA

M.R. Adams, L. Apanasevich, V.E. Bazterra, R.R. Betts, I. Bucinskaite, J. Callner, R. Cavanaugh, O. Evdokimov, L. Gauthier, C.E. Gerber, D.J. Hofman, S. Khalatyan, P. Kurt, D.H. Moon, C. O'Brien, C. Silkworth, D. Strom, P. Turner, N. Varelas

The University of Iowa, Iowa City, USA

U. Akgun, E.A. Albayrak⁵², B. Bilki⁶⁰, W. Clarida, K. Dilsiz, F. Duru, J.-P. Merlo, H. Mermerkaya⁶¹, A. Mestvirishvili, A. Moeller, J. Nachtman, H. Ogul, Y. Onel, F. Ozok⁵², S. Sen, P. Tan, E. Tiras, J. Wetzel, T. Yetkin⁶², K. Yi

Johns Hopkins University, Baltimore, USA

B.A. Barnett, B. Blumenfeld, S. Bolognesi, G. Giurgiu, A.V. Gritsan, G. Hu, P. Maksimovic, C. Martin, M. Swartz, A. Whitbeck

The University of Kansas, Lawrence, USA

P. Baringer, A. Bean, G. Benelli, R.P. Kenny III, M. Murray, D. Noonan, S. Sanders, R. Stringer, J.S. Wood

Kansas State University, Manhattan, USA

A.F. Barfuss, I. Chakaberia, A. Ivanov, S. Khalil, M. Makouski, Y. Maravin, L.K. Saini, S. Shrestha, I. Svintradze

Lawrence Livermore National Laboratory, Livermore, USA

J. Gronberg, D. Lange, F. Rebassoo, D. Wright

University of Maryland, College Park, USA

A. Baden, B. Calvert, S.C. Eno, J.A. Gomez, N.J. Hadley, R.G. Kellogg, T. Kolberg, Y. Lu, M. Marionneau, A.C. Mignerey, K. Pedro, A. Peterman, A. Skuja, J. Temple, M.B. Tonjes, S.C. Tonwar

Massachusetts Institute of Technology, Cambridge, USA

A. Apyan, G. Bauer, W. Busza, I.A. Cali, M. Chan, L. Di Matteo, V. Dutta,

G. Gomez Ceballos, M. Goncharov, D. Gulhan, Y. Kim, M. Klute, Y.S. Lai, A. Levin, P.D. Luckey, T. Ma, S. Nahn, C. Paus, D. Ralph, C. Roland, G. Roland, G.S.F. Stephans, F. Stöckli, K. Sumorok, D. Velicanu, R. Wolf, B. Wyslouch, M. Yang, Y. Yilmaz, A.S. Yoon, M. Zanetti, V. Zhukova

University of Minnesota, Minneapolis, USA

B. Dahmes, A. De Benedetti, A. Gude, J. Haupt, S.C. Kao, K. Klapoetke, Y. Kubota, J. Mans, N. Pastika, R. Rusack, M. Sasseville, A. Singovsky, N. Tambe, J. Turkewitz

University of Mississippi, Oxford, USA

J.G. Acosta, L.M. Cremaldi, R. Kroeger, S. Oliveros, L. Perera, R. Rahmat, D.A. Sanders, D. Summers

University of Nebraska-Lincoln, Lincoln, USA

E. Avdeeva, K. Bloom, S. Bose, D.R. Claes, A. Dominguez, M. Eads, R. Gonzalez Suarez, J. Keller, I. Kravchenko, J. Lazo-Flores, S. Malik, F. Meier, G.R. Snow

State University of New York at Buffalo, Buffalo, USA

J. Dolen, A. Godshalk, I. Iashvili, S. Jain, A. Kharchilava, A. Kumar, S. Rappoccio, Z. Wan

Northeastern University, Boston, USA

G. Alverson, E. Barberis, D. Baumgartel, M. Chasco, J. Haley, A. Massironi, D. Nash, T. Orimoto, D. Trocino, D. Wood, J. Zhang

Northwestern University, Evanston, USA

A. Anastassov, K.A. Hahn, A. Kubik, L. Lusito, N. Mucia, N. Odell, B. Pollack, A. Pozdnyakov, M. Schmitt, S. Stoynev, K. Sung, M. Velasco, S. Won

University of Notre Dame, Notre Dame, USA

D. Berry, A. Brinkerhoff, K.M. Chan, M. Hildreth, C. Jessop, D.J. Karmgard, J. Kolb, K. Lannon, W. Luo, S. Lynch, N. Marinelli, D.M. Morse, T. Pearson, M. Planer, R. Ruchti, J. Slaunwhite, N. Valls, M. Wayne, M. Wolf

The Ohio State University, Columbus, USA

L. Antonelli, B. Bylsma, L.S. Durkin, S. Flowers, C. Hill, R. Hughes, K. Kotov, T.Y. Ling, D. Puigh, M. Rodenburg, G. Smith, C. Vuosalo, B.L. Winer, H. Wolfe, H.W. Wulsin

Princeton University, Princeton, USA

E. Berry, P. Elmer, V. Halyo, P. Hebda, J. Hegeman, A. Hunt, P. Jindal, S.A. Koay,

P. Lujan, D. Marlow, T. Medvedeva, M. Mooney, J. Olsen, P. Piroué, X. Quan, A. Raval, H. Saka, D. Stickland, C. Tully, J.S. Werner, S.C. Zenz, A. Zuranski

University of Puerto Rico, Mayaguez, USA

E. Brownson, A. Lopez, H. Mendez, J.E. Ramirez Vargas

Purdue University, West Lafayette, USA

E. Alagoz, D. Benedetti, G. Bolla, D. Bortoletto, M. De Mattia, A. Everett, Z. Hu, M. Jones, K. Jung, O. Koybasi, M. Kress, N. Leonardo, D. Lopes Pegna, V. Maroussov, P. Merkel, D.H. Miller, N. Neumeister, I. Shipsey, D. Silvers, A. Svyatkovskiy, F. Wang, W. Xie, L. Xu, H.D. Yoo, J. Zablocki, Y. Zheng

Purdue University Calumet, Hammond, USA

N. Parashar

Rice University, Houston, USA

A. Adair, B. Akgun, K.M. Ecklund, F.J.M. Geurts, W. Li, B. Michlin, B.P. Padley, R. Redjimi, J. Roberts, J. Zabel

University of Rochester, Rochester, USA

B. Betchart, A. Bodek, R. Covarelli, P. de Barbaro, R. Demina, Y. Eshaq, T. Ferbel, A. Garcia-Bellido, P. Goldenzweig, J. Han, A. Harel, D.C. Miner, G. Petrillo, D. Vishnevskiy, M. Zielinski

The Rockefeller University, New York, USA

A. Bhatti, R. Ciesielski, L. Demortier, K. Goulios, G. Lungu, S. Malik, C. Mesropian

Rutgers, The State University of New Jersey, Piscataway, USA

S. Arora, A. Barker, J.P. Chou, C. Contreras-Campana, E. Contreras-Campana, D. Duggan, D. Ferencek, Y. Gershtein, R. Gray, E. Halkiadakis, D. Hidas, A. Lath, S. Panwalkar, M. Park, R. Patel, V. Rekovic, J. Robles, S. Salur, S. Schnetzer, C. Seitz, S. Somalwar, R. Stone, S. Thomas, P. Thomassen, M. Walker

University of Tennessee, Knoxville, USA

K. Rose, S. Spanier, Z.C. Yang, A. York

Texas A&M University, College Station, USA

O. Bouhali⁶³, R. Eusebi, W. Flanagan, J. Gilmore, T. Kamon⁶⁴, V. Khotilovich, R. Montalvo, I. Osipenkov, Y. Pakhotin, A. Perloff, J. Roe, A. Safonov, T. Sakuma, I. Suarez, A. Tatarinov, D. Toback

Texas Tech University, Lubbock, USA

N. Akchurin, C. Cowden, J. Damgov, C. Dragoiu, P.R. Dudero, K. Kovitanggoon, S.W. Lee, T. Libeiro, I. Volobouev

Vanderbilt University, Nashville, USA

E. Appelt, A.G. Delannoy, S. Greene, A. Gurrola, W. Johns, C. Maguire, Y. Mao, A. Melo, M. Sharma, P. Sheldon, B. Snook, S. Tuo, J. Velkovska

University of Virginia, Charlottesville, USA

M.W. Arenton, S. Boutle, B. Cox, B. Francis, J. Goodell, R. Hirosky, A. Ledovskoy, C. Lin, C. Neu, J. Wood

Wayne State University, Detroit, USA

S. Gollapinni, R. Harr, P.E. Karchin, C. Kottachchi Kankanamge Don, P. Lamichhane, A. Sakharov

University of Wisconsin, Madison, USA

D.A. Belknap, L. Borrello, D. Carlsmith, M. Cepeda, S. Dasu, S. Duric, E. Friis, M. Grothe, R. Hall-Wilton, M. Herndon, A. Hervé, P. Klabbers, J. Klukas, A. Lanaro, R. Loveless, A. Mohapatra, I. Ojalvo, T. Perry, G.A. Pierro, G. Polese, I. Ross, T. Sarangi, A. Savin, W.H. Smith, J. Swanson

†: Deceased

1: Also at Vienna University of Technology, Vienna, Austria

2: Also at CERN, European Organization for Nuclear Research, Geneva, Switzerland

3: Also at Institut Pluridisciplinaire Hubert Curien, Université de Strasbourg, Université de Haute Alsace Mulhouse, CNRS/IN2P3, Strasbourg, France

4: Also at National Institute of Chemical Physics and Biophysics, Tallinn, Estonia

5: Also at Skobeltsyn Institute of Nuclear Physics, Lomonosov Moscow State University, Moscow, Russia

6: Also at Universidade Estadual de Campinas, Campinas, Brazil

7: Also at California Institute of Technology, Pasadena, USA

8: Also at Laboratoire Leprince-Ringuet, Ecole Polytechnique, IN2P3-CNRS, Palaiseau, France

9: Also at Zewail City of Science and Technology, Zewail, Egypt

10: Also at Suez Canal University, Suez, Egypt

11: Also at Cairo University, Cairo, Egypt

12: Also at Fayoum University, El-Fayoum, Egypt

13: Also at British University in Egypt, Cairo, Egypt

14: Now at Ain Shams University, Cairo, Egypt

- 15: Also at National Centre for Nuclear Research, Swierk, Poland
- 16: Also at Université de Haute Alsace, Mulhouse, France
- 17: Also at Universidad de Antioquia, Medellin, Colombia
- 18: Also at Joint Institute for Nuclear Research, Dubna, Russia
- 19: Also at Brandenburg University of Technology, Cottbus, Germany
- 20: Also at The University of Kansas, Lawrence, USA
- 21: Also at Institute of Nuclear Research ATOMKI, Debrecen, Hungary
- 22: Also at Eötvös Loránd University, Budapest, Hungary
- 23: Also at Tata Institute of Fundamental Research - EHEP, Mumbai, India
- 24: Also at Tata Institute of Fundamental Research - HECR, Mumbai, India
- 25: Now at King Abdulaziz University, Jeddah, Saudi Arabia
- 26: Also at University of Visva-Bharati, Santiniketan, India
- 27: Also at University of Ruhuna, Matara, Sri Lanka
- 28: Also at Isfahan University of Technology, Isfahan, Iran
- 29: Also at Sharif University of Technology, Tehran, Iran
- 30: Also at Plasma Physics Research Center, Science and Research Branch, Islamic Azad University, Tehran, Iran
- 31: Also at Università degli Studi di Siena, Siena, Italy
- 32: Also at Centre National de la Recherche Scientifique (CNRS) - IN2P3, Paris, France
- 33: Also at Purdue University, West Lafayette, USA
- 34: Also at Universidad Michoacana de San Nicolas de Hidalgo, Morelia, Mexico
- 35: Also at INFN Sezione di Padova; Università di Padova; Università di Trento (Trento), Padova, Italy
- 36: Also at Faculty of Physics, University of Belgrade, Belgrade, Serbia
- 37: Also at Facoltà Ingegneria, Università di Roma, Roma, Italy
- 38: Also at Scuola Normale e Sezione dell'INFN, Pisa, Italy
- 39: Also at University of Athens, Athens, Greece
- 40: Also at Paul Scherrer Institut, Villigen, Switzerland
- 41: Also at Institute for Theoretical and Experimental Physics, Moscow, Russia
- 42: Also at Albert Einstein Center for Fundamental Physics, Bern, Switzerland
- 43: Also at Gaziosmanpasa University, Tokat, Turkey
- 44: Also at Adiyaman University, Adiyaman, Turkey
- 45: Also at Cag University, Mersin, Turkey
- 46: Also at Mersin University, Mersin, Turkey
- 47: Also at Izmir Institute of Technology, Izmir, Turkey
- 48: Also at Ozyegin University, Istanbul, Turkey
- 49: Also at Kafkas University, Kars, Turkey

-
- 50: Also at Suleyman Demirel University, Isparta, Turkey
51: Also at Ege University, Izmir, Turkey
52: Also at Mimar Sinan University, Istanbul, Istanbul, Turkey
53: Also at Kahramanmaras Sütcü Imam University, Kahramanmaras, Turkey
54: Also at Rutherford Appleton Laboratory, Didcot, United Kingdom
55: Also at School of Physics and Astronomy, University of Southampton, Southampton, United Kingdom
56: Also at INFN Sezione di Perugia; Università di Perugia, Perugia, Italy
57: Also at Utah Valley University, Orem, USA
58: Also at Institute for Nuclear Research, Moscow, Russia
59: Also at University of Belgrade, Faculty of Physics and Vinca Institute of Nuclear Sciences, Belgrade, Serbia
60: Also at Argonne National Laboratory, Argonne, USA
61: Also at Erzincan University, Erzincan, Turkey
62: Also at Yildiz Technical University, Istanbul, Turkey
63: Also at Texas A&M University at Qatar, Doha, Qatar
64: Also at Kyungpook National University, Daegu, Korea